LA-8336-MS

c. 3



# Criticality Calculations and Criticality Monitoring Studies of the Slagging Pyrolysis Incinerator Facility



LOS ALAMOS SCIENTIFIC LABORATORY
Post Office Box 1663 Los Alamos, New Mexico 87545

Edited by

Christine L. B. Siciliano

Photocomposition by

Chris West and Joni Lee Powell

This work was supported by the US Department of Energy, Transuranic Waste Management Programs and Idaho National Engineering Laboratory.



**UNITED STATES**
**DEPARTMENT OF ENERGY**
**CONTRACT W-7405-ENG. 36**

LA-8336-MS

UC-46
Issued: January 1981

# Criticality Calculations and Criticality Monitoring Studies of the Slagging Pyrolysis Incinerator Facility

D. A. Close
T. E. Booth
J. T. Caldwell

## CONTENTS

# CRITICALITY CALCULATIONS AND CRITICALITY MONITORING STUDIES OF THE SLAGGING PYROLYSIS INCINERATOR FACILITY

by

D. A. Close, T. E. Booth, and J. T. Caldwell

## ABSTRACT

We determined that the criticality hazard associated with the Slagging Pyrolysis Incinerator (SPI) Facility proposed by Idaho National Engineering Laboratory would be minimal if a three-level criticality-hazard prevention program were implemented. The first strategy consists of screening all incoming wastes for fissile content. An estimate of the average fissile content of wastes to be processed by the SPI Facility is $\leq$1 g fissile per 50 kg waste. Monte Carlo calculations indicate that under normal operating conditions this average fissile concentration poses no criticality hazard. A fissile concentration in the SPI Facility ten times this average value is required to produce k of about 0.4. Large lumps are not allowed to enter the system, which effectively prevents a rapidly developing criticality hazard. Suitable instrumentation to easily and reliably accomplish this screening/assay is currently under development at both EG&G, Inc. and Los Alamos Scientific Laboratory.

The second prevention level is provided by introducing a small concentration of a neutron-absorbing compound, such as $B_2O_3$, into the input waste stream. Our Monte Carlo calculations showed, for instance, that including only $1.0 \times 10^{-2}$ wt fraction of $B_2O_3$ reduces the criticality hazard to a negligible level.

*Example:* For 9.3 kg $^{239}$Pu in the drying region without $B_2O_3$, k = 0.99. For the same 9.3 kg of $^{239}$Pu in the drying region with $1.0 \times 10^{-2}$ wt fraction of $B_2O_3$ added, k = 0.24.

The third prevention level is provided by direct criticality-hazard monitoring using sensitive neutron detectors in all regions of the facility where a significant hazard has been identified—principally the drying, pyrolysis, and slag regions. These detectors can be operated in a passive mode or can be used with a pulsed external neutron source to obtain a direct measure of k. These neutron detectors have been used in other applications to measure k in the range 0.05 to 0.10. They can also be used to determine an approximate value of the total fissile mass in the SPI Facility. On the basis of this data, the facility could be shut down rapidly for cleanout if these measurements indicate an unsafe condition is developing. The criticality safety provided by the product of these three independent measures should reduce the hazard to a negligible level. We recommend that they be implemented in the SPI Facility. A detailed fault tree statistical analysis should be done to quantify the safety factors associated with each of the three levels of this criticality-hazard prevention program. Such an analysis is beyond the scope of this report.

---

## INTRODUCTION

The Los Alamos Scientific Laboratory (LASL) study of the proposed Slagging Pyrolysis Incinerator (SPI) Facility for criticality hazard and for appropriate criticality monitoring was initiated at the request of EG&G, Inc., Idaho Falls, Idaho. LASL agreed to independently study the problem of criticality hazard in the SPI Facility and to recommend, on the basis of this study, appropriate criticality-monitoring instrumentation and/or procedures to minimize or lessen potential criticality hazards.

Specific analyses for this study included the following.

I. A Monte Carlo neutron study was performed to (1) examine the effects of neutron poisoning and various typical matrix materials on criticality, as well as their effects on possible criticality-monitoring systems; (2) identify areas of the SPI Facility where criticality hazards exist; and (3) quantify the hazards as much as possible. Specifically, we addressed the problems associated with plutonium lumps being processed through the system and quantified the criticality hazards associated with plating out of plutonium in various regions.

II. A study of direct criticality-monitoring techniques and equipment included both active and passive neutron-based methods, with a limited number of experimental measurements on multiplying systems. Recommendations of the appropriate technique(s) with estimates of needed development and associated costs were included.

III. The general problem of distinguishing between fissile and fertile materials in waste both before and after slagging was studied.

IV. Methods for assaying product slag in 91.44-cm-(36-in.-) diam x 30.48-cm-(12-in.-) thick ingots were studied.

## I. MONTE CARLO NEUTRON CALCULATIONS OF THE CRITICALITY HAZARD IN THE SPI FACILITY

### A. Section Summary

Monte Carlo calculations were performed to determine critical plutonium concentrations in various regions of the proposed SPI Facility. The incinerator was divided into three plutonium-containing regions: the drying, pyrolysis, and slag regions. Calculations indicated that these regions are only weakly coupled neutronically; that is, when each region by itself is close to critical, the whole incinerator remains close to critical. The critical plutonium weight fractions for the drying, pyrolysis, and slag forming regions are $3.0 \times 10^{-3}$, $2.6 \times 10^{-3}$, and $2.0 \times 10^{-2}$, respectively. These weight fractions translate into $^{239}Pu$ critical masses of 9.3, 28.7, and 271 kg, respectively. In other words, the minimum critical mass of $^{239}Pu$ for the SPI Facility as a whole is 9.3 kg if the entire 9.3 kg is placed within the drying region.

Under some operating conditions, fissile material build-up within the SPI Facility is possible. In this situation, a criticality hazard could potentially develop even though only average fissile content waste was being processed. A strategy to lessen this hazard is to mix a small amount of neutron absorbing material into the waste. Calculations indicated, for example, that $1.0 \times 10^{-2}$ wt fraction of $B_2O_3$ mixed with the waste greatly reduces the criticality hazard associated with any given fissile inventory. This fraction of $B_2O_3$ uniformly mixed with an otherwise critical concentration of plutonium in the drying region reduces k to about 0.24, a reasonably safe value. In fact, a similar strategy is used routinely to prevent criticality hazards in fissile-containing solutions. Here neutron absorption is provided by placing borosilicate glass "raschig" rings within the solution.[1]

Such dramatic effects might not be obtained under all conditions with $1.0 \times 10^{-2}$ wt fraction of $B_2O_3$; however, it is clear that this simple procedure produces a highly cost effective reduction in overall criticality hazard. In contrast, designing boron into the gasifier structure itself does not have a large effect on criticality. Calculationally, k of the hearth region drops from 1.00 to 0.76 when the firebrick is totally replaced with natural elemental boron.

Calculations indicated that fissile lumps (administratively defined as single inclusions of $\geq$200 g fissile) can produce a rapidly developing criticality hazard. A single 200-g lump of high density $^{239}PuO_2$ can result in k of 0.21, whereas the same $^{239}PuO_2$ mass spread uniformly throughout the drying region produces k about 0.05. Fissile lumps should not be processed in the SPI Facility because they could conceivably lead to a rapidly developing criticality hazard.

### B. Introduction

An SPI Facility has been proposed by the Idaho National Engineering Laboratory (INEL) for processing their stored transuranic (TRU) wastes. Figure 1 is a

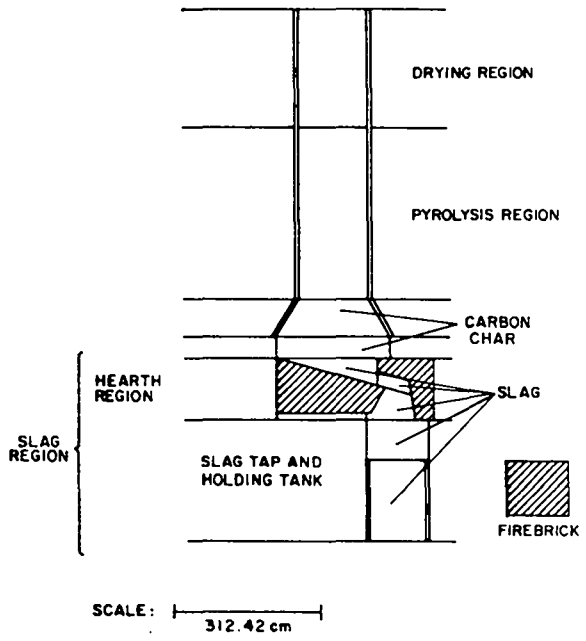


Fig. 1.
**Calculational geometry of the SPI, showing the yz plane at x = 0. Shown are the drying, pyrolysis, and slag regions. The slag region is composed of two smaller regions—the hearth region and the slag tap and holding tank.**

simplified drawing of the incinerator that is used for calculational purposes. The plutonium-contaminated wastes enter the incinerator in the drying region, pass through the pyrolysis region, and then enter the slag region where the wastes are heated to a molten mass. This incinerator model was studied for criticality hazards.

These extensive Monte Carlo calculations used LASL's Monte Carlo code for neutron and photon transport (MCNP).[2] Specifically, MCNP was used to calculate k of the incinerator. The k of a system is defined as the multiplication factor of the system. The different regions of the incinerator—drying, pyrolysis, and slag—were studied individually and as a total system. The k of each of the three regions was calculated as a function of the $^{239}Pu$ concentration. As discussed below, the drying region of the incinerator has the lowest critical mass of $^{239}Pu$ of the three regions. For this region, the effect of neutron poisons, namely boron in the form $B_2O_3$, on k of this region was studied. Another specialized case studied was the build-up of a layer of $^{239}PuO_2$ on the walls of the drying and pyrolysis regions. The input material to the SPI Facility even after screening could conceivably contain 200-g lumps of $^{239}PuO_2$. The effect of such a lump of $^{239}PuO_2$ in the drying region on k of the region was calculated also.

Part of our analysis of the SPI Facility included possible methods for monitoring the neutron activity in the incinerator. Additional neutronic calculations modeled neutron detectors surrounding the incinerator to determine the effect of increased moderation resulting from the neutron detectors.

Initial parameter studies indicated the SPI Facility had a positive temperature coefficient; k increases as the temperature increases. The final series of calculations for the incinerator determined the variation of k on the temperature of the drying region, a not insignificant effect.

Three secondary structures associated with the SPI Facility were also studied. These were the secondary combustion chamber, slag tap, and holding tank; the tundish; and the off-gas collection hopper.

All calculations were performed assuming plutonium to be the fissile material. This is justified because the anticipated amount of highly enriched uranium to be processed by the SPI Facility is a small fraction of the anticipated amount of plutonium to be processed. All other parameters being equal, the critical mass, concentration, or volume of $^{239}Pu$ is less than or equal to that for $^{233,235}U$. Thus, results obtained for plutonium translate into corresponding conservative $^{235}U$ or $^{233}U$ results.

## C. Brief Code Description

The general-purpose MCNP[2] code can be used for neutron, photon, or coupled neutron-photon transport, which includes the capability to calculate eigenvalues of critical systems. The code treats an arbitrary three-dimensional configuration of materials in geometric cells that can be specified by first- and second-degree surfaces and some special fourth-degree surfaces (elliptical tori).

Pointwise cross-section data are used. For neutrons, all reactions given in a particular cross-section evaluation (such as ENDF/B-IV) are accounted for. Thermal neutrons are described by both the free gas and $S(\alpha,\beta)$ models. For photons, the code takes account of incoherent and coherent scattering, the possibility of fluorescent emission following photoelectric absorption, and absorption in pair production with local emission of annihilation radiation.

Standard features that are available to improve computation efficiency include geometry splitting and Russian roulette, weight cutoff with Russian roulette, correlated sampling, analog capture or capture by weight reduction, exponential transformation, energy splitting, forced collisions in designated cells, flux estimates at point or ring detectors, deterministically transporting pseudo-particles to designated regions, track-length estimators, source biasing, and several parameter cutoffs.

Extensive summary information is provided in the computer listing to help the user better understand the physics and Monte Carlo simulation of his problem. The standard, user-defined output of MCNP includes two-way current as a function of direction across any set of surfaces or surface segments in the problem. Flux across any set of surfaces or surface segments is computed. Similarly, the flux at designated detectors and the average flux in any cell (track length per unit volume) are standard tallies. Reactions such as fission, tritium production, absorption, or any product of the flux times any standard ENDF reaction cross section plus several nonstandard ones may be obtained in any cell, at a surface, or at a point. The heating tallies give the energy deposition in designated cells. In addition, particles may be flagged when they cross specified surfaces or enter designated cells, and the contributions of these flagged particles to the tallies are listed separately. The user is allowed to modify any of the standard tallies almost at will. All quantities tallied also have their relative errors calculated. All tallies are a function of time and energy as defined by the user.

MCNP has the capability to calculate eigenvalues for both sub- and supercritical systems. The calculation is run as a series of generations of neutrons. At the end of each generation, $k_{eff}$ is calculated for that generation as well as averaged over a specified number of preceding generations. The source for the first generation is usually defined by the user at a set of spatial points in the system. The neutrons are then started isotropically at these points with an energy sampled from standard fission distributions.

The cross sections used were taken from several sources. If an ENDF/B cross-section file was available for the isotope of interest, it was chosen as the preferred cross section. Some of the ENDF/B cross-section files were version III and some were version IV. Alternative cross-section files were taken as needed from LLL-Howerton.

### D. Material Compositions and Region Temperatures

Tables I-VI list the elemental compositions of the materials in the different regions of the incinerator and the secondary structures. All elemental compositions are given as weight percentages. The elemental composition of the material in the drying region[3] is listed in Table I. The density of this material is 0.706 g/cm$^3$. The material in the pyrolysis region[3] has a density of 1.76 g/cm$^3$, and its elemental composition is presented in Table II. The slag material is common to the slag region (hearth, slag tap, and holding tank) of the incinerator; the secondary combustion chamber, slag tap, and holding tank; and the tundish. The slag has a density of 2.80 g/cm$^3$, and its elemental composition[3] is given in Table III. A large fraction of the external surface area of the slag-forming region in the incinerator is surrounded by firebrick. There is also firebrick surrounding the slag in the secondary combustion chamber, slag tap, and holding tank, and in the tundish. The elemental composition of the firebrick,[3] which has a density of 2.70 g/cm$^3$, is listed in Table IV. The composition of type 316 stainless steel on the outside of the tundish and surrounding the off-gas collection hopper is presented in Table V. The elemental composition of the material in the off-gas collection hopper[4] is given in Table VI. One of the compounds in this material was a trace metal oxide, which we assumed to be stainless steel, knowing plutonium-contaminated stainless steel would be part of the feed material for the SPI Facility.

None of the above tables indicates the presence of plutonium. The plutonium concentration, expressed as a weight percentage, was a variable, and different amounts were added to the drying, pyrolysis, slag, and off-gas collection materials.

Except for the stainless steel, none of the material compositions adds to 100%. This is because the information provided us did not add to 100% and because the plutonium concentration is not included in the tables.

Another parameter needed by MCNP is the temperature of each material and region. At elevated temperatures, neutron resonances become wider because of Doppler broadening effects. Such an effect changes the neutron interaction cross section. Because of relatively high temperatures in the slag and the firebrick, it was deemed advisable to use appropriate temperatures. The temperatures provided by INEL[4] for the different regions of the incinerator and for the secondary structures are presented in Table VII.

TABLE I

DRYING REGION MATERIAL ELEMENTAL COMPOSITION[a,b]

| Element | Weight Percent |
|---|---|
| H | 4.99 |
| C | 25.10 |
| O | 48.54 |
| Na | 0.57 |
| Al | 1.62 |
| Si | 8.15 |
| S | 0.80 |
| Ca | 2.02 |
| Fe | 6.86 |
| | 98.65 |

[a]Density = 0.706 g/cm$^3$
[b]Ref. 3.

TABLE II

PYROLYSIS REGION MATERIAL ELEMENTAL COMPOSITION[a,b]

| Element | Weight Percent |
|---|---|
| H | 3.53 |
| C | 1.41 |
| O | 42.30 |
| Na | 1.41 |
| Mg | 1.06 |
| Al | 4.23 |
| Si | 21.20 |
| K | 1.41 |
| Ca | 5.29 |
| Ti | 0.03 |
| Mn | 0.46 |
| Fe | 17.60 |
| | 99.93 |

[a]Density= 1.76 g/cm$^3$
[b]Ref. 3.

TABLE III

SLAG REGION; SECONDARY COMBUSTION CHAMBER, SLAG TAP, AND HOLDING TANK; AND TUNDISH MATERIAL ELEMENTAL COMPOSITION[a,b]

| Element | Weight Percent |
|---|---|
| C | 1.30 |
| O | 45.80 |
| Na | 1.41 |
| Mg | 1.04 |
| Al | 4.12 |
| Si | 21.10 |
| K | 1.32 |
| Ca | 5.20 |
| Mn | 0.50 |
| Fe | 17.90 |
| | 99.69 |

[a]Density = 2.80 g/cm$^3$
[b]Ref. 3.

TABLE IV

FIREBRICK ELEMENTAL COMPOSITION[a,b]

| Element | Weight Percent |
|---|---|
| O | 49.70 |
| Na | 0.74 |
| Mg | 0.60 |
| Al | 20.10 |
| Si | 26.30 |
| Ca | 0.71 |
| Ti | 1.20 |
| Fe | 0.71 |
| | 100.06 |

[a]Density = 2.70 g/cm$^3$
[b]Ref. 3.

TABLE V

TYPE 316 STAINLESS STEEL ELEMENTAL COMPOSITION[a]

| Element | Weight Percent |
|---|---|
| Cr | 18.5 |
| Fe | 68.5 |
| Ni | 13.0 |
| | 100.0 |

[a]Density = 8.02 g/cm$^3$

TABLE VI

OFF-GAS COLLECTION HOPPER MATERIAL ELEMENTAL COMPOSITION[a,b]

| Element | Weight Percent |
|---|---|
| C | 1.25 |
| O | 37.56 |
| Na | 15.51 |
| Mg | 0.36 |
| Al | 3.23 |
| Si | 21.32 |
| S | 1.42 |
| Cl | 13.41 |
| K | 0.58 |
| Ca | 1.43 |
| Cr | 0.55 |
| Fe | 3.01 |
| Ni | 0.28 |
| | 99.91 |

[a]Density = 1.28 g/cm$^3$
[b]Ref. 4.

TABLE VII

TEMPERATURE OF REGIONS OF INCINERATOR[a]

| Region | Temperature (°C) |
|---|---|
| Drying | 1000 |
| Pyrolysis | 1000 |
| Slag | 1482 |
| Firebrick | 1260 |
| Water Jacket | 66 |
| Tundish | 1482 |
| Secondary Combustion Chamber | 1482 |
| Off-Gas Collection Hopper | 149 |

[a]Ref. 4.

## E. Incinerator Geometry

Figure 1 is a view of the incinerator[5] as modeled for the MCNP criticality calculations. Labeled are the drying, pyrolysis, and slag regions. The slag region includes the hearth region and the slag tap and holding tank. The hearth region contains the burners and is almost totally surrounded by firebrick. The area between the hearth and the pyrolysis regions is filled with carbonaceous char having a density of 2.1 g/cm$^3$. There is a 7.62-cm-(3-in.-) thick water jacket surrounding the drying and pyrolysis regions. The slag tap and holding tank area is surrounded by a 5.08-cm-(2-in.-) thick layer of firebrick and a 2.54-cm-(1-in.-) thick water jacket. The drying region is a cylinder having a radius of 73.66 cm (29 in.) and a height of 256.54 cm (101 in.). The cylindrical pyrolysis region has a radius of 73.66 cm (29 in.) and a height of 368.30 cm (145 in.). The slag tap and holding tank area has a radius of 60.96 cm (24 in.) and a height of 267.64 cm (105.37 in.). Other dimensions can be obtained from the scale indicated on the figure. A complete description of the geometry is presented in the Appendix.

Criticality calculations are usually performed using a greatly simplified geometry, replacing complicated structures with much simpler, critically conservative approximations. This approach was not used in this analysis. An accurate geometrical model was used for the entire SPI Facility. This analysis should more accurately predict the neutronic behavior of the facility as various neutronic perturbations are applied to the incinerator. It must be emphasized that this is a very complicated geometry for MCNP calculations. Considerable computer time is required to obtain a converged source for k calculations. We feel that the 10- to 15-min calculations done for this study, resulting in a 2% std dev on k, are sufficient to allow work to proceed on the SPI Facility. However, several 1- to 2-h calculations should be done when the plans are complete to obtain a better

## TABLE VIII

## SPI FACILITY k CALCULATIONS

| Case | Drying Region | k |
|---|---|---|
| 1 | $7.5 \times 10^{-4}$ wt fraction $^{239}Pu$ | 0.49 |
| 2 | $1.5 \times 10^{-3}$ wt fraction $^{239}Pu$ | 0.74 |
| 3 | $3.0 \times 10^{-3}$ wt fraction $^{239}Pu$ | 0.99 |
| 4 | $4.65 \times 10^{-3}$ wt fraction $^{239}Pu$ | 1.16 |
| 5 | $3.0 \times 10^{-3}$ wt fraction Pu (6% $^{240}Pu$) | 0.96 |
| | **Pyrolysis Region** | |
| 6 | $6.5 \times 10^{-4}$ wt fraction $^{239}Pu$ | 0.47 |
| 7 | $1.3 \times 10^{-3}$ wt fraction $^{239}Pu$ | 0.74 |
| 8 | $2.2 \times 10^{-3}$ wt fraction $^{239}Pu$ | 0.95 |
| 9 | $2.6 \times 10^{-3}$ wt fraction $^{239}Pu$ | 1.02 |
| | **Slag Region** | |
| 10 | $2.0 \times 10^{-3}$ wt fraction $^{239}Pu$ | 0.57 |
| 11 | $5.0 \times 10^{-3}$ wt fraction $^{239}Pu$ | 0.77 |
| 12 | $2.0 \times 10^{-2}$ wt fraction $^{239}Pu$ | 0.99 |
| | **Slag Tap and Holding Tank** | |
| 13 | $2.0 \times 10^{-2}$ wt fraction $^{239}Pu$ | 0.86 |
| 14 | $3.0 \times 10^{-2}$ wt fraction $^{239}Pu$ | 0.92 |
| 15 | $5.0 \times 10^{-2}$ wt fraction $^{239}Pu$ | 1.00 |
| 16 | $5.0 \times 10^{-1}$ wt fraction $^{239}Pu$; 100% boron instead of firebrick | 0.92 |
| 17 | $2.0 \times 10^{-2}$ wt fraction $^{239}Pu$; increased firebrick density 10X | 1.04 |
| 18 | $2.0 \times 10^{-2}$ wt fraction $^{239}Pu$; 5 g/cm$^3$ $H_2O$ in water jacket | 0.96 |
| | **Hearth Region** | |
| 19 | $2.0 \times 10^{-2}$ wt fraction $^{239}Pu$ | 1.00 |
| 20 | $2.0 \times 10^{-2}$ wt fraction $^{239}Pu$; 100% boron instead of firebrick | 0.76 |
| | **Critical Conc. of $^{239}Pu$ in Each Region** | |
| 21 | $3.0 \times 10^{-3}$ wt fraction in drying region, $2.6 \times 10^{-3}$ wt fraction in pyrolysis region, and $2.0 \times 10^{-2}$ wt fraction in slag region | 0.99 |

| Case | Drying Region with $3.0 \times 10^{-3}$ wt fraction $^{239}Pu$ | k |
|---|---|---|
| 22 | $1.0 \times 10^{-3}$ wt fraction $B_2O_3$ in drying region | 0.77 |
| 23 | $1.0 \times 10^{-2}$ wt fraction $B_2O_3$ in drying region | 0.24 |
| 24 | 5 g/cm$^3$ $H_2O$ in water jacket | 1.01 |
| 25 | 100% boron in water jacket | 0.96 |
| 26 | increased $H_2O$ in drying region from 25 wt% to 37.5 wt% | 0.98 |
| | **1-cm Layer $^{239}PuO_2$ in Drying and Pyrolysis Regions $\rho$ ($^{239}PuO_2$) = 11.5 g/cm$^3$** | |
| 27 | no other $^{239}Pu$ in incinerator | 0.97 |
| 28 | 100% boron in water jacket; no other $^{239}Pu$ | 0.80 |
| 29 | 5 g/cm$^3$ $H_2O$ in water jacket; no other $^{239}Pu$ | 1.02 |
| | **200-g, 1.61-cm-Radius, Spherical Lump $^{239}PuO_2$ in Drying Region $\rho$ ($^{239}PuO_2$) = 11.5 g/cm$^3$** | |
| 30 | $3.0 \times 10^{-3}$ wt fraction $^{239}Pu$ in drying region | 0.98 |
| 31 | no other $^{239}Pu$ in incinerator | 0.21 |
| | **$3.0 \times 10^{-3}$ wt fraction $^{239}Pu$ in Drying Region** | |
| 32 | 500°C drying temperature, all other temperatures at standard values | 0.88 |
| 33 | 750°C | 0.96 |
| 34 | 1000°C | 1.01 |
| 35 | 1170°C | 1.00 |
| 36 | 1500°C | 1.03 |
| | **Off-Gas Collection Hopper** | |
| 37 | $5.0 \times 10^{-1}$ wt fraction $^{239}Pu$ | 1.02 |
| | **Tundish** | |
| 38 | $4.0 \times 10^{-3}$ wt fraction $^{239}Pu$ | 0.97 |
| | **Secondary Combustion Chamber, Slag Tap, and Holding Tank** | |
| 39 | $2.0 \times 10^{-2}$ wt fraction $^{239}Pu$ | 0.86 |
| 40 | $4.0 \times 10^{-2}$ wt fraction $^{239}Pu$ | 0.97 |
| 41 | $5.0 \times 10^{-2}$ wt fraction $^{239}Pu$ | 1.03 |

converged source and to obtain a higher degree of confidence in the results.

### F. Results

The results of the MCNP k calculations are presented in Table VIII. Unless noted otherwise, all calculations were made for $^{239}Pu$. All k values have a 2% std dev associated with them. Cases 1-5 give the variation of k with plutonium concentration in the drying region of the incinerator. The calculation in Case 5 was made using weapons-grade plutonium (94% $^{239}Pu$, 6% $^{240}Pu$) in the drying region. The variation of k with the plutonium concentration in the pyrolysis region is given in Cases 6-9. Studies of the slag region, slag tap and holding tank, and hearth region are summarized in Cases 10-20. Included in these slag region studies are the effects of changing the external neutron moderators. Case 21 had critical concentrations of $^{239}Pu$ everywhere.

Some calculations were made to study the effects of adding neutron absorbing material to the feed mixture on the critical concentrations of $^{239}Pu$. These studies were done only for the most critically sensitive region, the drying region, and are summarized in Cases 22 and 23. The effect of external neutron moderators on the neutronics of the drying region is listed in Cases 24 and 25. Case 26 indicates what happens to k when the amount of water in the drying region is increased from 25 to 37.5 wt%, keeping the weight fraction of $^{239}Pu$ constant.

A potential nonstandard operating situation is the build-up of a layer of plutonium on the inside surface of the drying and pyrolysis regions. A very conservative estimate was made assuming this layer to be $^{239}PuO_2$ of density 11.5 g/cm$^3$. The results of the calculations for a layer of $^{239}PuO_2$ are presented in Cases 27-29.

The feed material for the SPI Facility could contain lumps of plutonium having a mass up to 200 g. The effects of a 200-g lump of $^{239}PuO_2$ ($\rho = 11.5$ g/cm$^3$) on k of the drying region are presented in Cases 30 and 31.

Calculations indicated that k is sensitive to the temperature of the region. Cases 32-36 summarize the variation of k with the temperature of the drying region.

The last five entries in Table VIII, Cases 37-41, are the results of calculations on the off-gas collection hopper (Case 37), the tundish (Case 38), and the secondary combustion chamber, slag tap, and holding tank (Cases 39-41).

## G. Discussion of Incinerator Results

Figure 2 shows the variation of k with $^{239}Pu$ concentration in the drying region of the incinerator. The drying region has a critical $^{239}Pu$ concentration of $3.0 \times 10^{-3}$ wt fraction. This is equivalent to a mass of 9.3 kg $^{239}Pu$. When the plutonium concentration decreases by a factor of 2, k of the system drops to 0.74. Another decrease by a factor of 2 in the plutonium concentration decreases k to 0.49.

Because the drying region has the lowest critical $^{239}Pu$ mass, this region was used to study matrix effects. The SPI Facility will be processing stored wastes that are contaminated mainly with weapons-grade plutonium. Consequently, a calculation was made to determine the effect of 6% $^{240}Pu$. The result of this calculation is shown in Fig. 2, detailing the variation of k in the drying region with plutonium concentration. This calculation assumed a critical concentration of plutonium, $3.0 \times 10^{-3}$ wt fraction. Weapons-grade plutonium lowers k of the drying region by about 3%. Plutonium-240 has a fission threshold of about 1 MeV; thermal neutrons can fission $^{239}Pu$. The drying region is 5 wt% hydrogen or 45% atom fraction hydrogen. Thus the drying region is heavily moderated, and the neutrons rapidly lose energy. Neutrons are not able to fission $^{240}Pu$ and there is less $^{239}Pu$ in the region. Consequently, k of the region decreases.

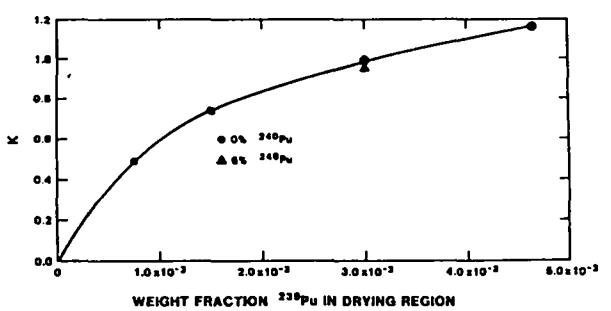


Fig. 2.
Variation of k for the drying region with the weight fraction of $^{239}Pu$ in the drying region. ● = $^{239}Pu$; ▲ = 94% $^{239}Pu$, 6% $^{240}Pu$. The size of the data points includes the 2% std dev on the calculations. The curve merely serves to guide the eye.

Another matrix study increased the amount of water in the drying region. One class of stored wastes is sludge drums containing a large amount of water. The effect of additional water on k of the drying region needed to be quantified. The drying region is normally 25 wt% water. The amount of water in the drying region was arbitrarily increased by 50% to a total value of 37.5 wt%. The k of the drying region under this situation is 0.98. The increase in water did not substantially change k of the region. (The difference is within the standard deviation on the MCNP calculations.) The initial hydrogen density in the drying region thermalizes most of the fast fission neutrons. Adding hydrogen does not produce any substantial additional thermalization.

The effect of adding neutron absorbers on k of the drying region was another matrix study. Varying amounts of $B_2O_3$ (natural isotopic composition) were added to the material in the drying region. For this series of calculations, the $^{239}Pu$ concentration in the drying region was held fixed at the critical concentration, $3.0 \times 10^{-3}$ wt fraction. Figure 3 summarizes the effect of adding $B_2O_3$ to the material in the drying region. A $1.0 \times 10^{-3}$ wt fraction of $B_2O_3$ reduces k from 0.99 to 0.77. A $1.0 \times 10^{-2}$ wt fraction of $B_2O_3$ reduces k to 0.24. A small amount of natural boron added to the feed material appears to be a very effective technique for controlling the criticality of the SPI Facility. When a $1.0 \times 10^{-2}$ wt

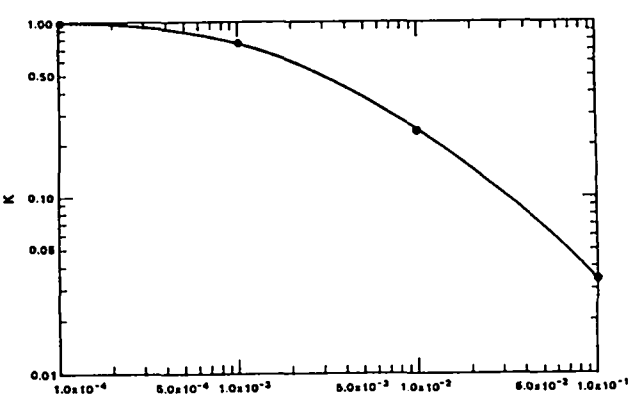


Fig. 3.
Effect of adding $B_2O_3$ to the drying region on k of the drying region. The size of the data points includes the 2% std dev on the calculations. The curve merely serves to guide the eye.

fraction of $B_2O_3$ is in the feed mixture, the neutron spectrum that would be incident on a detector is somewhat harder, and there are about 15% fewer neutrons emerging from the drying region. For heavily moderated $^3He$ tubes, the boron will probably cause about a 15% change in the expected signal.

The feed material for the drying region could contain lumps of plutonium. The maximum permissible loading of plutonium in a 208-$\ell$ (55-gal.) drum is 200 g. A critically conservative approach for these studies considered a 200-g spherical lump of $^{239}PuO_2$ with the theoretical density of 11.5 g/cm$^3$. Such a sphere of $^{239}PuO_2$ has a radius of 1.61 cm. The size of this sphere is very small compared to the volume of the drying region of the SPI Facility. For MCNP to adequately sample this small volume of $^{239}PuO_2$, special importance sampling techniques were used. Two calculations were performed on the lump of $^{239}PuO_2$. One calculation assumed the lump was in the drying region; the region had a critical $^{239}Pu$ concentration of 3.0 x $10^{-3}$ wt fraction. Without the lump, k of the region is 0.99; with the 200-g lump of $^{239}PuO_2$, k of the region is 0.98. No effect outside the 2% std dev on the calculations was observed. The other calculation on the 200-g lump of $^{239}PuO_2$ assumed there was no other $^{239}Pu$ in the drying region. This situation has k = 0.21. Additional criticality calculations must be performed if lumps of plutonium having a mass larger than 200 g are to be allowed in the feed material.

The use of an external neutron absorber to control the criticality was studied by replacing the water in the water jacket surrounding the drying region with natural boron. A critical $^{239}Pu$ concentration of 3.0 x $10^{-3}$ wt fraction was in the region. Using external means to control criticality is very ineffective. The boron reduced k of the system from 0.99 to 0.96, not a statistically significant change.

The effect external neutron detectors would have on the neutronics of the SPI Facility was studied also. The assumption was made that thermal neutron detectors would be used to monitor criticality. Thus there would be slabs of polyethylene or other efficient neutron moderators surrounding the incinerator. These external moderators were modeled by increasing the density of the water in the water jackets. No attempt was made to take into account that neutrons would be absorbed in the detectors. This is a conservative approach. Increasing the density of water in the water jacket surrounding the drying region changed k for this region from 0.99 to 1.01. This change is not statistically significant.

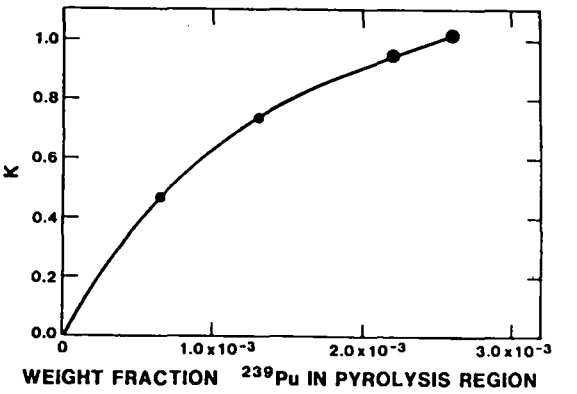


Fig. 4.
Variation of k for the pyrolysis region with the weight fraction of $^{239}Pu$ in the pyrolysis region. The size of the data points includes the 2% std dev on the calculations. The curve merely serves to guide the eye.

The variation of k with $^{239}Pu$ concentration in the pyrolysis region is shown in Fig. 4. The pyrolysis region has a critical $^{239}Pu$ concentration of 2.6 x $10^{-3}$ wt fraction. This is equivalent to a mass of 28.7 kg $^{239}Pu$. A decrease by a factor of 2 in the $^{239}Pu$ concentration reduces k to 0.74. Another decrease by a factor of 2 in the $^{239}Pu$ concentration further reduces k to 0.47. This is the same relative behavior as observed in the drying region.

A conservative approximation was made of the effect of plutonium build-up on the inside surfaces of the drying and pyrolysis regions on k of the system. This is an abnormal operating condition. The layer of plutonium was $^{239}PuO_2$ (theoretical density $\rho$ = 11.5 g/cm$^3$). Any actual layer of $^{239}PuO_2$ on the inside surfaces would probably have a density closer to 2.0 g/cm$^3$. The plating of plutonium on the inside surfaces of the incinerator does not create a criticality hazard per se. Our calculations indicate that a large mass of plutonium (10's of kg) plated on the inside surfaces is required to create a significant criticality hazard. Build-ups of this magnitude would be detected by the neutron detectors surrounding the incinerator long before any hazard develops. The real criticality hazard is the potential of this layer of plutonium breaking up and falling down into the incinerator. Nine kilograms of plutonium uniformly distributed in the drying region is critical. Using the neutron detectors discussed below, 9 kg can be detected on the walls of the incinerator. Assuming a safe operating condition of k $\cong$ 0.20, 800 g can be plated on the walls, and a criticality hazard will not develop if that quantity falls into the incinerator, even if all the material coalesces into one lump.

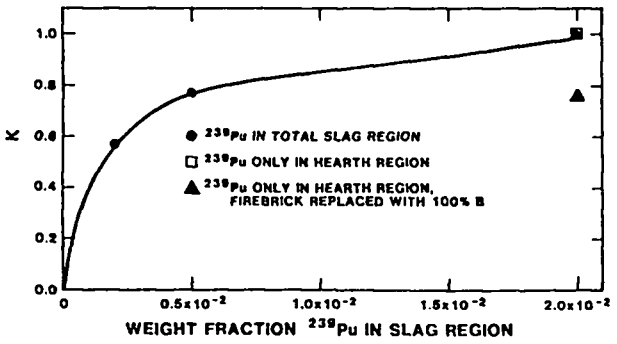


Fig. 5.

Dependence of k on the weight fraction of $^{239}Pu$ in the slag region. The size of the data points includes the 2% std dev on the calculations. The curve merely serves to guide the eye. ● = $^{239}Pu$ in the total slag region. For the critical concentration 2.0 x $10^{-2}$ wt fraction, k was calculated for $^{239}Pu$ only in the hearth region (□) and for $^{239}Pu$ only in the hearth region with the firebrick surrounding the hearth replaced with 100% natural boron (▲).

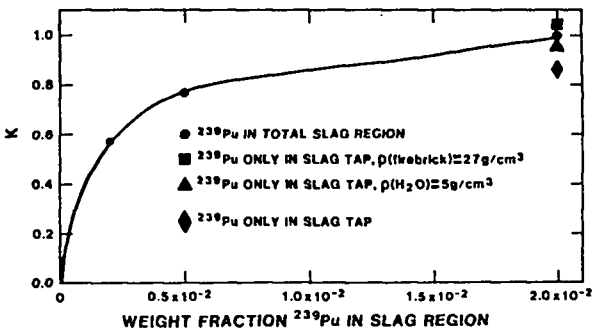


Fig. 6.

Dependence of k on the weight fraction of $^{239}Pu$ in the slag region. The size of the data points includes the 2% std dev on the calculations. The curve merely serves to guide the eye. ● = $^{239}Pu$ in the total slag region. Additional calculations were made for the critical concentration 2.0 x $10^{-2}$ wt fraction. The ◆ gives k for $^{239}Pu$ only in the slag tap. The ▲ gives k when there is only $^{239}Pu$ in the slag tap, and the density of water in the water jacket surrounding the slag tap has been increased by a factor of 5. The ■ gives k for $^{239}Pu$ only in the slag tap when the density of the firebrick surrounding the slag tap has been increased by a factor of 10.

Figure 5 shows the variation of k with $^{239}Pu$ concentration in the slag region. The slag region has a critical $^{239}Pu$ concentration of 2.0 x $10^{-2}$ wt fraction. This is equivalent to a mass of 271 kg $^{239}Pu$. For the slag region, a decrease by a factor of 4 in the $^{239}Pu$ concentration reduces k to 0.77. A further decrease by a factor of 2.5 in the $^{239}Pu$ concentration reduces k to 0.57. Thus the slag region is not as sensitive to changes in $^{239}Pu$ concentration as are the drying and pyrolysis regions. However, it is expected that the 1.0 x $10^{-2}$ wt fraction of $B_2O_3$ placed in the slag region will make a similar reduction in k as it did in the drying region. For these calculations of k, total blockage to the level of the burners was assumed. The critical mass of the slag region is so large mainly because of the slag tap and holding tank. Blueprints of the slag tap and holding tank had a dimension labeled "as required," which was assumed to be 85 cm.

Several studies for the slag region were made because sampling problems were observed when the entire region was treated as a whole. Subsequent calculations were made only on the hearth region and only on the slag tap and holding tank area. (See Fig. 1 for a definition of these regions.) Figure 5 compares the results for the hearth region with those for the total slag region. The comparison is for a single $^{239}Pu$ concentration, 2.0 x $10^{-2}$ wt fraction. This weight fraction is critical for the total slag region, and there is no difference in k for the hearth region and the total slag region. The hearth region has a critical mass of about 80 kg $^{239}Pu$. When the firebrick is replaced totally with natural boron, k of the hearth region drops significantly to 0.76.

The comparison between the total slag region and the slag tap and holding tank only is shown in Fig. 6. When a 2.0 x $10^{-2}$ wt fraction of $^{239}Pu$ is present only in the slag tap and holding tank, k of the incinerator is 0.86. For this same concentration in the total slag region, k = 0.99. Thus k of the total slag region is effectively k of the hearth region which is the most reactive region. To a certain extent, the hearth region is neutronically isolated from the slag tap and holding tank. This is partially due to a feature of the calculational model. The blueprints of the slag tap region had a dimension "as required." As this dimension is increased, the two regions of the slag become more isolated.

The k of the slag tap and holding tank is lower because of the absence of adequate neutron moderators surrounding the slag tap and holding tank. They are surrounded by only 5.08-cm-(2-in.-) thick firebrick and a 2.54-cm-(1-in.-) water jacket. When the density of the water in the water jacket surrounding the slag tap and holding tank is artificially increased fivefold, k increases to 0.96. This effect increases the neutron moderation near the surface of the slag tap and holding tank and increases the number of fissions near the surface. Artificially increasing the density of the water also simulates the effect of a thermal neutron detector,

heavily moderated with water or polyethylene, used to monitor activity in the slag tap and holding tank region.

The effect of external neutron moderators was established also by artificially increasing the density of the firebrick surrounding the slag tap and holding tank. A tenfold increase in the firebrick density increases k to 1.04. The effect of external moderators around the slag tap and holding tank is so noticeable because the slag does not have any efficient neutron moderators in it. The interior of the slag tap and holding tank appears to be an infinite medium, but the outer few centimeters of the slag tap and holding tank are easily influenced by external moderators.

After the critical $^{239}Pu$ concentration of each region was determined, a calculation was made on the entire incinerator with each region having a critical concentration of $^{239}Pu$ in it. The k of the entire system was 0.99. Within the 2% std dev on the calculations, there is no difference between calculating k for each region separately and calculating k for the entire incinerator. There is little neutron transfer between the different regions. Neutronically, each region appears to be independent. We are thus justified in treating each region separately.

Figure 7 summarizes the temperature effect on the incinerator, specifically the drying region. The drying region has an operating temperature of 1000°C. For the calculations summarized here, the temperature of this region was varied from 500 to 1500°C. The temperatures of all other regions were held fixed at the values listed in Table VII. For all temperature calculations, the drying region had a $^{239}Pu$ concentration of $3.0 \times 10^{-3}$ wt fraction, a critical concentration when the temperature is 1000°C. The k of the drying region varies from a low of $0.88 \pm 0.02$ for T = 500°C to a high of $1.03 \pm 0.02$ for T = 1500°C. There is a noticeable rise in k as the temperature rises from 500 to 1000°C. For temperatures above 1000°C, k is much less sensitive to changes in temperature. As the temperature rises from 1000 to 1500°C, k varies within the 2% std dev on the calculations. Because the drying region operates at 1000°C, any increase in temperature should produce only small fluctuations in k. Any decrease in operating temperature from 1000°C decreases k. These calculations emphasize the need to use correct temperatures for the different regions of the incinerator and for the cross-section evaluation because of the considerable Doppler broadening effects on neutron resonances.

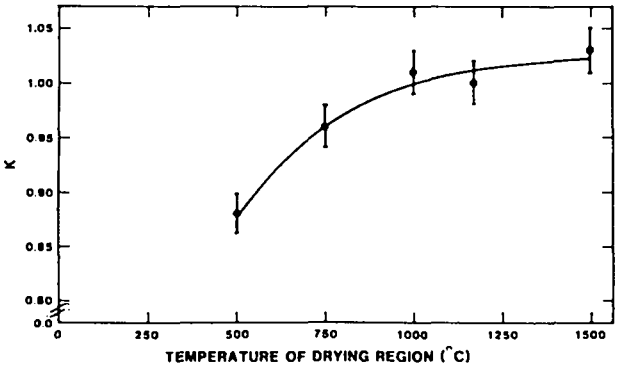


Fig. 7.
Variation of k with the temperature of the drying region, which contained a $3.0 \times 10^{-3}$ wt fraction of $^{239}Pu$. The curve merely serves to guide the eye.

## H. Secondary Combustion Chamber, Slag Tap, and Holding Tank

The calculational model of the secondary combustion chamber, slag tap, and holding tank[6] is shown in Fig. 8. The secondary combustion chamber, slag tap, and holding tank has cylindrical symmetry. The lower region is surrounded by a 5.08-cm-(2-in.-) thick firebrick, which is surrounded by a 2.54-cm-(1-in.-) thick water jacket. The compositions of the slag material and the firebrick were presented in Tables III and IV, respectively. Figure 9 shows the placement of materials in the secondary combustion chamber. From Table VIII, the calculated critical $^{239}Pu$ weight fraction in the secondary combustion chamber, slag tap, and holding tank is between $4.0 \times 10^{-2}$ and $5.0 \times 10^{-2}$. This is equivalent to a mass between 450 and 560 kg $^{239}Pu$. This $^{239}Pu$ weight fraction is to be compared with a $2.0 \times 10^{-2}$ critical wt fraction of $^{239}Pu$ in the slag region. The secondary combustion chamber, slag tap, and holding tank unit does not have as much moderating material around it as does the slag (hearth) region. Consequently, the critical concentration of $^{239}Pu$ in the secondary combustion chamber, slag tap, and holding tank is greater than that in the slag region.

## I. Tundish

The tundish[4] is a parallelepiped with dimensions 426.72 cm (168 in.) x 365.76 cm (144 in.) x 213.36 cm (84 in.) high. The bottom and sides are surrounded by a 60.96-cm-(24-in.-) thick firebrick. Surrounding the firebrick is a 5.08-cm-(2-in.-) thick type 316 stainless steel

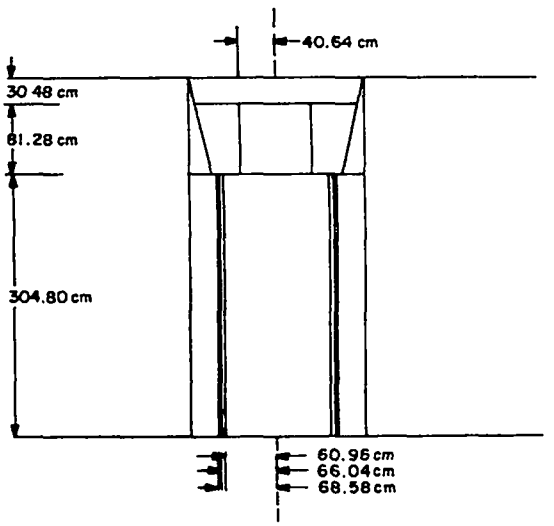


Fig. 8.
*Calculational geometry of the secondary combustion chamber, slag tap, and holding tank. Appropriate dimensions of important regions are given.*

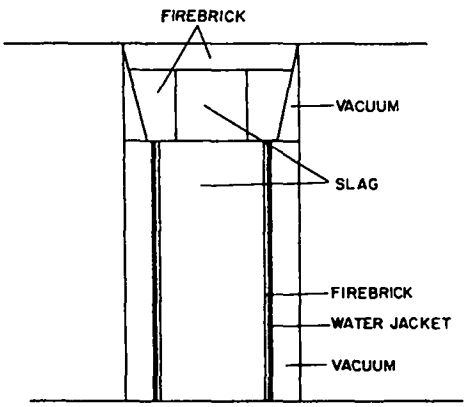


Fig. 9.
*Material regions in the secondary combustion chamber, slag tap, and holding tank.*

jacket. The material in the tundish is identical to that in the slag region of the incinerator, which was presented in Table III. Initially, the tundish would be expected to behave neutronically similar to the slag region and the secondary combustion chamber, slag tap, and holding tank. However, the critical $^{239}Pu$ concentration in the tundish is an order of magnitude less (see Table VIII). The critical wt fraction in the tundish is $4.0 \times 10^{-3}$. This is equivalent to 370 kg $^{239}Pu$. The slag does not have any efficient neutron moderators in it. The interior of the tundish appears infinite to the neutrons and thus is not affected by surrounding material. This is not true of the slag material near the outside edges of the tundish. The tundish is surrounded on five sides by firebrick and has more moderating material around it than does the slag region of the incinerator or the secondary combustion chamber. The firebrick surrounding the tundish is thick enough to moderate and reflect neutrons into the tundish. These reflected neutrons are of the right energy to fission the $^{239}Pu$ near the edges of the tundish, enhancing the fission rate and lowering the critical $^{239}Pu$ concentration.

## J. Off-Gas Collection Hopper

The off-gas collection hopper[4] is a 152.40-cm-(60-in.-) diam, 182.88-cm-(72-in.-) high cylinder. The walls of the collection hopper are 0.48-cm-(0.19-in.-) thick type 316 stainless steel. The composition of material in the collection hopper was presented in Table VI. The critical mass of $^{239}Pu$ in the collection hopper is calculated to be 50% by weight (see Table VIII). This is equivalent to a $^{239}Pu$ mass of 2140 kg, which initially seemed too large a mass. However, the material in the collection hopper does not contain any neutron moderators, and the collection hopper is not surrounded by neutron moderators. Several secondary calculations were made, artificially adding hydrogen to the composition. As the amount of hydrogen was increased, the critical mass of $^{239}Pu$ decreased. When the amount of hydrogen approached that in the drying or pyrolysis regions, a plutonium concentration similar to that in the drying or pyrolysis regions was calculated.

## K. Conclusions from Monte Carlo Studies

If only properly screened input material is processed, there does not appear to be a serious criticality hazard for the SPI Facility. The region having the largest criticality hazard is the drying region, where the critical mass of $^{239}Pu$ is 9.3 kg. The next most hazardous critical region would be the pyrolysis region, which has a critical mass of about 30 kg $^{239}Pu$. All other regions of the incinerator and secondary structures have critical masses greater than 200 kg $^{239}Pu$. Forty-five 208-$\ell$ (55-gal.) drums, each containing 200 g of plutonium, could be put into the SPI Facility at one time before causing a critical situation. This assumes that no build-up occurs.

The average plutonium concentration expected in the SPI Facility is 1 g plutonium per 50 kg waste. This is a wt

fraction of 2.0 x $10^{-5}$. There is no criticality problem in any region of the SPI Facility for this average waste. The drying region, which has the lowest critical mass, has a critical weight fraction that is one hundred times larger than that of the average waste. Other regions of the SPI Facility have critical weight fractions two-to-three orders of magnitude greater than that of the average waste.

However, one simple operation would greatly reduce any conceivable criticality hazard. A small amount of $B_2O_3$ (1.0 x $10^{-2}$ wt fraction) added to the feed mixture in the drying region reduces k from 0.99 to 0.24.

The addition of water to the feed material of the incinerator does not produce any statistically significant change in k of the drying region. Thermal neutron counters are expected to have minimal effects on the neutronics of the incinerator. Likewise, the use of external neutron absorbers to control k of the incinerator is not an effective technique. Such a technique has about a 20% maximum effect on k. To get this effect, either the water in the water jacket or the firebrick must be replaced totally with boron. Such changes are not possible because the water is needed for its cooling action, and the firebrick is needed for its thermal-insulating properties.

Lumps of plutonium, taken as 200 g or less of $^{239}PuO_2$, will not pose a criticality problem. It takes a large amount of plutonium build-up on the inside surfaces of the drying and pyrolysis regions to create a criticality hazard. However, the real criticality hazard with plutonium build-up develops if the layer of plutonium falls off the wall into the incinerator. Any plutonium build-up can be monitored by detectors surrounding the SPI Facility and alarms sounded long before any hazard develops.

The incinerator itself, excluding the tundish; secondary combustion chamber, slag tap, and holding tank; and off-gas collection hopper, has a positive temperature coefficient. An increase in the temperature of a region increases k of the region. This increase in k is most noticeable as the temperature in the drying region increases from 500 to 1000°C. Above 1000°C, k appears to level off with increasing temperature. The temperatures of the plutonium-containing regions are between 1000 and 1500°C. Thus changes in temperature should not produce large changes in k. For the drying region, an increase from 1000 to 1500°C changes k by at most 2%.

## II. DIRECT CRITICALITY MONITORING

### A. Section Summary

We define direct criticality monitoring as the measurement of radiation directly associated with the fissile material producing the criticality hazard. This is distinguished from indirect criticality monitoring, which uses the differences between input and output assays to infer residual fissile mass in the facility.

We examined both passive and active techniques for direct monitoring of system criticality, including total count rate, Feynman Variance, and Rossi-alpha. We identified, based on the very soft neutron spectrum emerging from the drying and pyrolysis regions, a particularly appropriate neutron detector design that can be used for both passive and active measurements. We calculated responses for these detection systems for efficiencies typical of the SPI Facility criticality monitoring geometry and demonstrated with measurements on several plutonium multiplying systems the feasibility of this type of monitoring system. If the criticality hazard is judged to be sufficiently serious in other regions of the SPI Facility, a similar neutron monitoring system can be easily installed and operated in those regions.

A passive neutron system should be adequate for direct criticality monitoring. The passive neutron data would be analyzed using both the total neutron count rate and a time-correlated analysis. The former provides a sensitive, very timely monitor of the system. A time-correlated analysis is used to minimize the interference from neutrons from matrix generated ($\alpha$,n) reactions. An upper limit alarm level can be set using the total count rate while the time-correlated analysis is used to determine, with a longer time constant, the actual system multiplication.

A compact pulsed neutron generator can be incorporated into the system. This feature allows both the system multiplication and the fissile material build-up to be determined. It is clearly a more complicated system than the passive system.

### B. Passive Neutron System

The MCNP calculations of the SPI Facility in Sec. I included neutron spectral output in the regions external to the drying and pyrolysis regions. These calculations

indicate a very soft neutron spectrum, produced primarily by interactions with hydrogen within these regions and in the water jacket surrounding them. Depending on the location, 1/3 to 1/2 of all neutrons in the potential detector region are near thermal energies. For this situation, an appropriate neutron detector is shown in Fig. 10. This design consists of an "open-faced sandwich" of $^3$He proportional counters and polyethylene. The bare portion of the $^3$He proportional counters faces the source and has a calculated efficiency[7] of about 95% for incident thermalized neutrons. The efficiency falls off rapidly with energy; the energy-averaged efficiency for the calculated drying/pyrolysis region spectrum is about 40-50%.

Because the neutron count rate is proportional to detector solid angle, the largest possible solid angle should be intercepted in the drying/pyrolysis regions. A 2-10% effective solid angle is possible, resulting in a $4\pi$ detection efficiency in the range of 1-5%.

The total passive neutron count rate can be used as a criticality monitor. Historically,[8,9] just such a system was used to monitor the state-of-the-system criticality in fast critical assembly research and development work. The typical SPI Facility waste matrix could produce

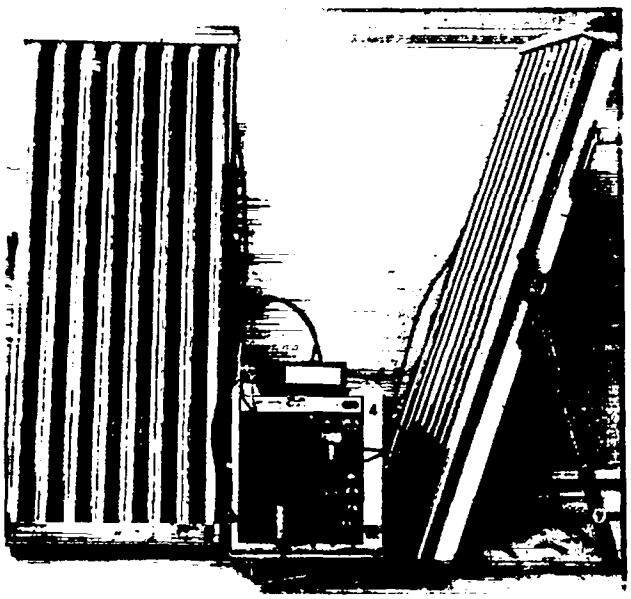

Fig. 10.
Typical set of $^3$He/polyethylene open-faced sandwich neutron detectors. This configuration is optimized for a highly moderated incident neutron spectrum.

(α,n) reactions. If a particular load of waste were to contain significant amounts of, for example, Be, B, or F (a very credible possibility[10]), then any TRU present can induce (α,n) reactions. Table IX (from Ref. 11) gives the measured neutron yields for typical TRU alpha particles incident on various materials with low atomic numbers.

A batch of waste containing modest amounts of plutonium combined with significant amounts of Be, B, or F could give a total neutron count rate that would appear to signal the presence of a significant criticality hazard. This would constitute a false alarm for a monitoring system based solely on the total neutron count rate.

Because the very nature of system multiplication guarantees a large number of time-correlated neutrons, one solution to the false alarm problem produced by (α,n) neutrons is time-correlation measurements. Many techniques have been devised to accomplish this.[12,13] Of particular applicability, however, is the Feynman or Reduced Variance technique.[14,15] This technique has been developed at LASL in connection with a Nuclear Emergency Search Team (NEST) requirement for portable system multiplication measurement equipment. A prototype module of such a system is shown in Fig. 11.

From an analysis of the basic physics of a multiplying system, one can show that[14]

$$Y = \text{const.} \frac{M\bar{\nu}\,(M\bar{\nu} - 1)}{\bar{\nu}^2} \quad , \tag{1}$$

TABLE IX

THICK TARGET NEUTRON YIELDS FOR 5.3-MeV ALPHA PARTICLES[a]

| Target Material | Observed Neutron Yield/$10^6$ α |
|---|---|
| Li | 2.60 |
| $O_2$ | 0.07 |
| Na | 1.50 |
| Mg | 1.40 |
| Al | 0.74 |
| Si | 0.16 |
| C | 0.11 |
| $F_2$ | 12.00 |
| B | 24.00 |
| Be | 80.00 |

[a]Ref. 11.

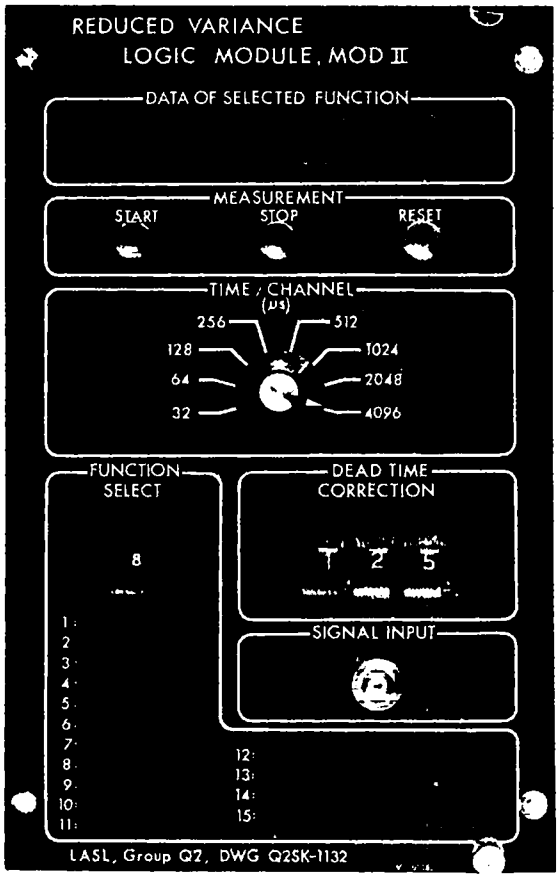


Fig. 11.
Front panel view of microprocessor-based Feynman Variance data collection/analysis module.

where M is the system multiplication, $\bar{\nu}$ is the average number of prompt neutrons emitted in a neutron-induced fission of the fissile material, and Y is a quantity generally defined as the "variance-to-mean ratio."

Experimentally,

$$Y = \frac{\overline{C^2} - \bar{C}^2}{\bar{C}} + \frac{2\bar{C}\tau}{T} - 1 \quad , \qquad (2)$$

where $\bar{C}$ is the experimentally measured average counts-per-random gate, T is the length of the randomly generated gates, $\overline{C^2}$ is the second moment of the observed distribution, and $\tau$ is a system deadtime. The system deadtime is measured experimentally by placing a time-uncorrelated source, such as an $(\alpha,n)$ source, near the detection system. For this source, $Y = 0$ and $\tau$ may be obtained.

In the experimental situation of a mixed $(\alpha,n)$ and fission source, the following quantity is useful.

$$Q = \overline{C^2} - \bar{C}^2 - \bar{C} + \frac{2\bar{C}^2\tau}{T} \quad . \qquad (3)$$

A comprehensive study (theoretical and experimental) of the general problem of mixed $(\alpha,n)$, spontaneous fission and system multiplication has been completed, and an initial report is being prepared.[16]

As a demonstration of the effectiveness of the Feynman Variance technique to determine system multiplication, we completed a series of measurements on some plutonium samples ranging in mass from about 0.5 to 4.0 kg. The cylindrical counting geometry was similar to that expected for an implemented neutron detection system in the SPI Facility around either the pyrolysis or drying regions. However, no attempt was made to mock up matrix effects for these measurements. That level of effort was beyond the scope of this study. These measurements serve to demonstrate the feasibility of the technique for plutonium masses of a size (as indicated by our MCNP calculations) that could be expected to result in significant system multiplication. This method is used routinely in the LASL NEST effort.

Figure 12 shows a plot of the basic experimental data with the quantity 1 + Y plotted as a function of plutonium mass. This results in a scatter plot with a

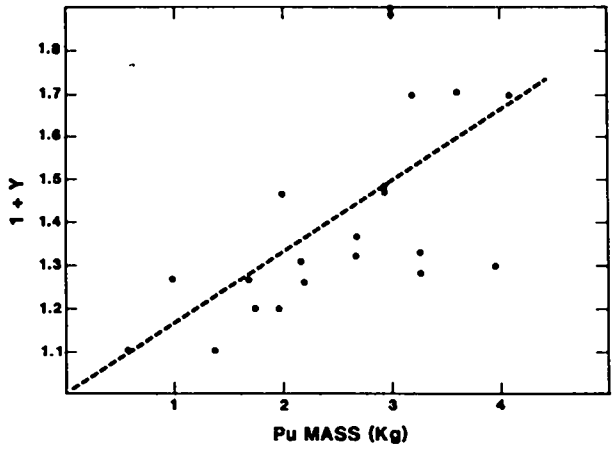


Fig. 12.
Feynman Variance data (1 + Y) obtained for a set of multiplying plutonium samples and plotted as a function of plutonium mass. Detection system used cylindrical geometry.

generally increasing trend as a function of increasing plutonium mass. The reason for the large scatter is that plutonium mass alone is not a good indicator of system multiplication. Some of these samples were spherical, some were cylindrical, and the sample density and $^{240}Pu$ isotopic content varied greatly.

When the same data are plotted differently (see Fig. 13), a very smooth curve results. Here 1 + Y is plotted as a function of the quantity Q ÷ $^{240}Pu$ mass. Dividing by the $^{240}Pu$ mass, which was known for all the samples, normalizes all samples according to the "driving source" present—$^{240}Pu$ spontaneous fission. If the samples were nonmultiplying, all would yield the same 1 + Y value. The actual system multiplication for each of the samples used was not determined independently. However, a MCNP calculation of the largest sample was made and indicated M ≅ 3.0 (or k ≅ 0.67). This corresponds to the largest 1 + Y value measured, about 1.9. Using this value to establish an approximate multiplication for the lowest 1 + Y value measured leads to an estimate of M ≅ 1.2 (k ≅ 0.17).

In Fig. 14, we show the calculated Feynman Variance quantity Q per fission as a function of system multiplication M for the anticipated range of 4π detection efficiencies. We would estimate the technique to be sensitive to k of 0.05-0.10 (M = 1.05-1.11).

To determine 1 + Y, we generally acquire data for $10^6$ random (but back-to-back) gates. The gate length must be matched to the detector/SPI Facility dieaway time. For the SPI Facility monitoring system, we estimate that T ≅ 1 ms is appropriate. This indicates a 1000-s count time is needed to acquire a typical set of data. However, for a fixed installation and use as a criticality monitor, a technique of time averaging would be appropriate. We have used this type of analysis successfully in other field instrumentation but not in the Feynman work. Here one could use a 1000-s analysis period, for instance, but update it more frequently. For example, a 1 + Y could be calculated every 5 or 10 s, with exclusion of the "oldest" 5 or 10 s of data and inclusion of the "newest" 5 or 10 s of data. If a significant change in 1 + Y occurs in the 5- or 10-s period, this would be reflected in the latest 1 + Y value because a few highly correlated events (neutron chains) would be weighted very strongly in the 1 + Y calculation. On the other hand, by retaining a relatively long total count time, much better counting statistics are obtained. This avoids the frequent false alarm problem that is always associated with poor counting statistics.

Another approach would be to set up a combined "AND" alarm system in which both a high 1 + Y value *and* a high total count rate are required before an alarm is sounded. This AND alarm approach has been used successfully at LASL. One can be sure that the most severe operational problem associated with a criticality monitor (or any other monitor) will be the false alarm problem. It is beyond the scope of this study to recommend a more specific solution to this false alarm problem. We believe, however, that the basic sensitivity

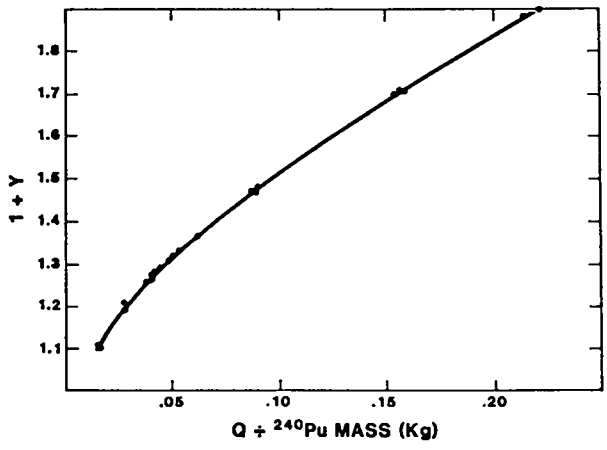


Fig. 13.
Same Feynman Variance data (1 + Y) as shown in Fig. 12 now plotted as a function of Q divided by $^{240}Pu$ mass.

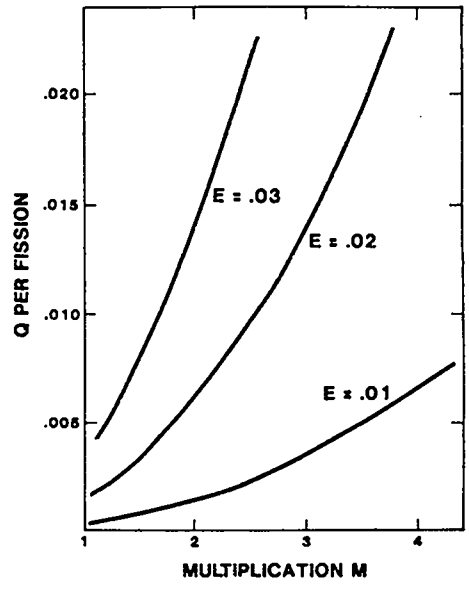


Fig. 14.
Calculated Feynman Variance quantity (Q per fission) as a function of system multiplication. The 4π detection efficiencies (0.01, 0.02, 0.03) are in the expected range for the SPI criticality monitoring system.

is well in hand with the $^{3}$He/polyethylene open-faced sandwich detectors and that some combination of total count rate and time-correlated (Feynman Variance) analysis will be sufficient. The analysis procedures are available at LASL and appropriate hardware exists. These are discussed in the references cited above.[12-16]

### C. Active Neutron System

If the passive neutron criticality monitor cannot provide a rapid enough response time, a pulsed active system might be required. Pulsed neutron sources based on the D + T reaction are commercially available[17] and have been used for various safeguards and activation analysis purposes. When the neutron correlation methods are reduced to their essence (Rossi-alpha, Feynman Variance), one finds that the pulsed neutron theory is identical to that used for a passive analysis. One measures various features of neutron multiplying chains, and it matters little if the initiating event occurs spontaneously or is induced.

The Rossi-alpha measurement generally involves measuring the prompt dieaway time of a multiplying assembly. The $^{3}$He/polyethylene open-faced sandwich neutron detectors discussed above are capable of monitoring the prompt dieaway time and could be used in an active pulsed mode. Fast recovery electronics are available (currently in use at LASL and elsewhere) for these detectors so that they can be operated in the presence of an interrogating pulsed source. One needs to keep open the active neutron option. A pulsed neutron generator of more than adequate neutron output ($1 \times 10^{6}$ n/pulse, 100 pps pulse rate) is currently available.[17] This system is quite small. It was designed to fit down small diameter boreholes for the oil well and uranium prospecting industries. Thus, it could be installed at the SPI Facility around the pyrolysis or drying region without occupying much space. Indeed, it is only slightly larger than a single $^{3}$He proportional counter.

## III. DISTINGUISHING BETWEEN FISSILE AND FERTILE MATERIALS IN NUCLEAR WASTE AT ALL STAGES

### A. Section Summary

Fissile material is best distinguished from fertile material by using assay techniques that are fissile specific. In this regard, techniques based on thermal neutron induced fission provide the solution. Such techniques specifically measure $^{235}$U, $^{239}$Pu, $^{241}$Pu, and other fissile isotopes, while giving no response for the common fertile isotopes, such as $^{238}$U. Techniques based on thermal neutron fission and directed specifically to measurements in typical waste matrices[17-19] are currently under development. One or more of these active neutron techniques should suffice to determine the fissile material content in the variety of wastes the SPI Facility is likely to encounter. These techniques can probably be developed to handle any particularly difficult matrix (such as sludges or concrete) in the leadtime available before the SPI Facility is scheduled to be operational.

As an adjunct to thermal neutron interrogation techniques, passive neutron coincidence methods can be used to quantify plutonium content in waste of reasonably well-characterized plutonium isotopic content, such as is the case for the bulk of the waste scheduled for processing in the SPI Facility. Photofission techniques are not easily applied to the general fissile assay problem. If unknown and significant amounts of $^{2}$H, $^{9}$Be, $^{13}$C, $^{17}$O, $^{238}$U, $^{232}$Th, or other isotopes that have low $(\gamma,n)$ thresholds or significant photofission yields are mixed in the waste, photofission techniques may indicate false positive fissile assay amounts. In some very dense matrices, however, photofission techniques may be needed. The assay problem is strongly matrix dependent. Continuing research and development efforts in this field will likely provide adequate solutions in the next few years.

### B. Active Thermal Neutron Fission Techniques

The nuclear safeguards groups at LASL have developed[18] a $^{252}$Cf neutron source, thermal neutron induced fission technique that is currently being specialized for use with 208-$\ell$ containers of high density nuclear waste. The technique, known as the "$^{252}$Cf Shuffler," consists of moving a strong ($10^{9}$-$10^{10}$ n/s) $^{252}$Cf neutron source into an interrogation cavity to induce fission reactions in any fissile material present and then removing it to a storage shield during a count cycle. Highly efficient $^{3}$He neutron counters are used to count delayed neutrons from the induced fissions during this part of the cycle. In test bed measurements at LASL using a 4.6 $\times$ $10^{8}$ n/s $^{252}$Cf source, a 3$\sigma$-detection limit (for a 700-s total irradiation/count period) of about 67 mg of $^{239}$Pu was determined. In scaled-up designs of this system

using a 10-25 times stronger $^{252}Cf$ source and a more efficient detection system, plutonium assay detection limits of about 4 mg have been projected.[18] A conceptual design of the $^{252}Cf$ Shuffler is shown in Fig. 15.

The LASL-EG&G/Santa Barbara waste assay workers are developing techniques based, in part, on neutron irradiation using a pulsed photoneutron source.[19] A pulse of photoneutrons is thermalized and used to irradiate a waste container around which is placed a $4\pi$ solid angle neutron detector. Following the irradiation, delayed neutrons from the induced fission reactions are counted. In a prototype 208-$\ell$ barrel-size detection system, a $3\sigma$-detection limit of a few milligrams of $^{239}Pu$ or $^{235}U$ has been obtained in a typical few 100's of seconds irradiation with photoneutrons produced by 10- to 18-MeV bremsstrahlung.

A technique[17] originally developed for use in the Enrichment Plant Safeguards Program at LASL is now under development for use in the Waste Management Program. This technique, called the "Differential Dieaway Technique (DDT)," uses pulses from a 14-MeV neutron generator as a source of ultimately thermalized neutrons. The generator is placed within a graphite-lined interrogation cavity (see Fig. 16), which is backed with polyethylene for additional neutron moderation, reflection, and personnel shielding. External to the graphite layer, but inside the bulk polyethylene layer, are fast-dieaway moderated $^{3}He$ neutron detectors. The neutronic properties of this system are shown in Fig. 17, which shows the thermalized neutron time history produced by a pulse from the neutron generator in (a) the external neutron detector, and (b) the interrogation cavity with a 208-$\ell$ barrel full of $\rho = 1.0$ g/cm$^3$ sand and vermiculite ($SiO_2$).

The original pulse of neutrons dies out rapidly in the external detector with no measureable response left after 0.4 to 0.5 ms. On the other hand, thermal neutrons dieaway in the interrogation cavity with a half-life of about 0.76 ms. (A lining of cadmium and boron neutron shielding totally isolates thermal neutrons from the external detector.) Thus, the interrogation pulse lasts a long time in the interrogation cavity and can induce thermal neutron fissions in any fissile material present in the waste barrel. Prompt fission neutrons (hard spectrum) from such reactions then propagate to the external detector where they are recorded.

Figure 18 shows the measured response for a 200-s interrogation period for samples of varying $^{235}U$ mass

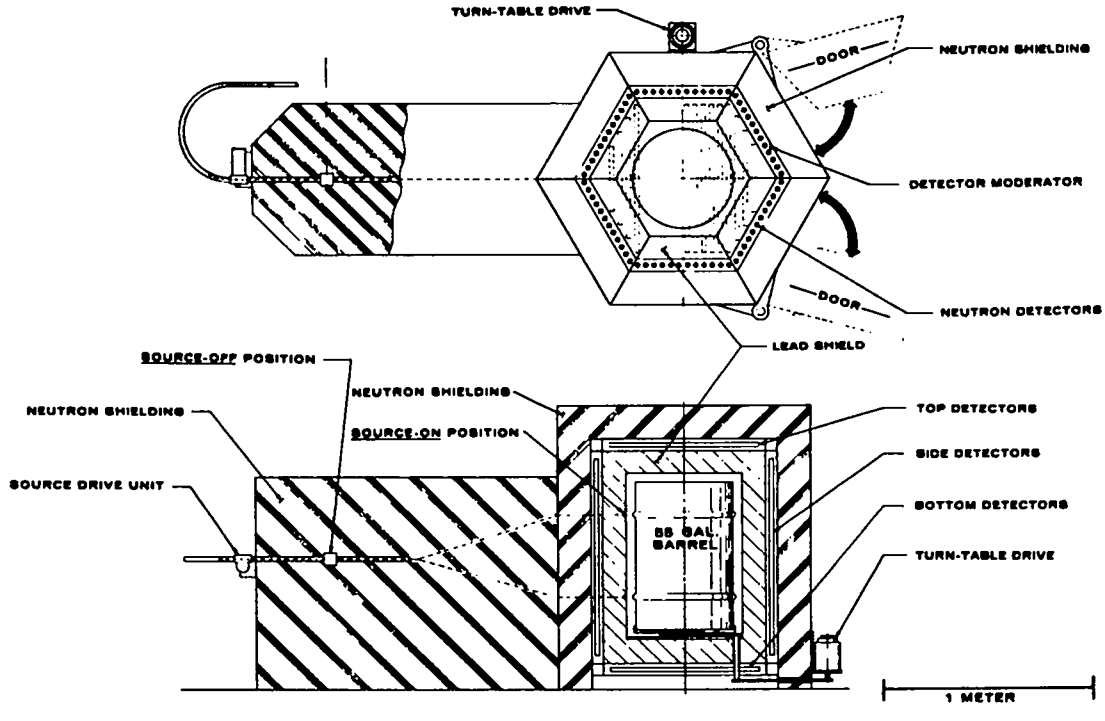


Fig. 15.
Conceptual design of 208-$\ell$ barrel-size $^{252}Cf$ Shuffler System.

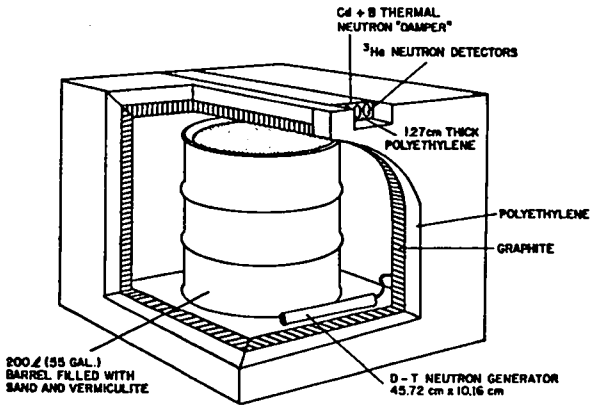


Fig. 16.
Schematic drawing of the prototype differential dieaway technique interrogation cavity and detector.

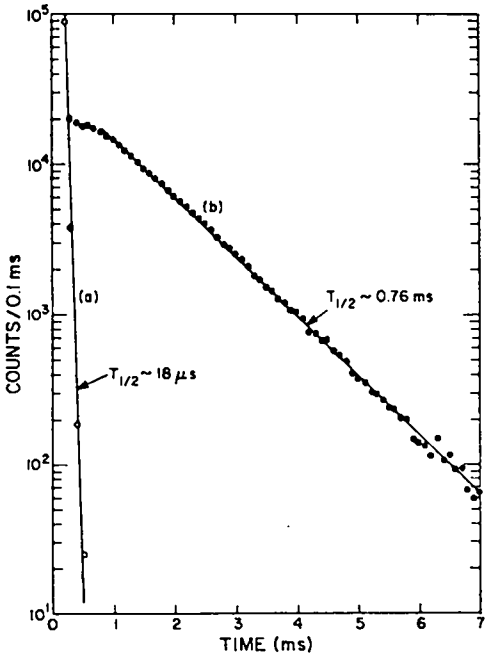


Fig. 17.
Pulsed neutron dieaway time data for (a) external detector and (b) interrogation cavity.

placed within the sand-/vermiculite-filled barrel. A linear response as a function of $^{235}$U mass was observed, with an indicated 3σ-detection limit of about 3-5 mg $^{235}$U for this prototype system. Additional studies[20] have shown a uniform (to ±10%) interrogation flux profile throughout the volume of the barrel as well. In other words, this

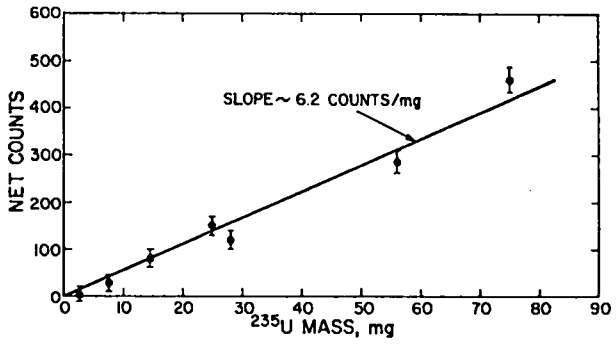


Fig. 18.
Experimental response (100-s data collection times) of differential dieaway technique prototype system as a function of $^{235}$U mass.

technique shows great promise for the assay of fissile material in low-level, high-density wastes.

Matrices consisting of high-hydrogen-density sludges or concrete will undoubtedly pose technical problems for some or all of the three techniques discussed above. Potential corrections to the analysis of this type of data do exist. If the matrix is known, standards or other techniques can be used to correct the analysis for the influence of the matrix. In particular, the DDT method involves the use of an interrogating flux monitor within the interrogation cavity.[17] Measurements done to date indicate that as the interrogating flux is absorbed or attenuated by waste matrix, the thermal neutron flux throughout the cavity is proportionately reduced. Thus, by simply dividing the external detector response by the internal cavity flux monitor, one effectively obtains an assay that compensates for matrix effects.

## C. Passive Neutron Assay Techniques

The Nuclear Safeguards Program[12,13] has long made extensive use of passive neutron coincidence techniques to quantify $^{240}$Pu content in a great variety of applications. With a known $^{240}$Pu isotopic ratio for the material being assayed, a complete total plutonium mass is simply calculated. For the proposed use of the SPI Facility,[10] the vast majority of the fissile content of the waste to be processed will consist of weapons-grade plutonium (5-6% $^{240}$Pu). In this situation, passive neutron coincidence counting techniques may play a large role.

A well-designed[18] 208-ℓ barrel-size passive neutron coincidence counting system is in the final design stage at

LASL. With it (when the system is properly shielded from the cosmic-ray background), one can obtain a plutonium assay sensitivity of about 100 mg for 5-6% $^{240}Pu$ content material in a 300-s assay.

In addition, work is progressing on a crate-size passive coincidence detector at LASL.[21] When completed and accompanied with appropriate cosmic-ray shielding, this detection system will have the capability of assaying 121.92-cm (48-in.) x 121.92-cm (48-in.) x 213.36-cm (84-in.) crates to an assay sensitivity of about 50-100 mg plutonium (5-6% $^{240}Pu$ content) in a 1000-s assay period. Depending on the physical size of the waste containers at the SPI Facility, one or the other of these passive systems may be useful.

### D. SPI Facility Input Screening

Waste screening will prevent many potential criticality problems. We recommend that it be based on assay measurements done *before* the waste enters the final process stream in the SPI Facility. We also recommend that such screening use the pulsed neutron generator DDT system. No matter what size the waste containers are, an applicable DDT system will be available within a few years.

This preliminary screening would sort waste into the broad categories of (1) average TRU content, waste that has an acceptable fissile content; (2) low TRU content, waste that is essentially fissile free (to be regarded as an asset and kept separate for blending purposes); and (3) high TRU content, waste that has an unacceptably high fissile content.

At this point the high TRU content waste fraction should be subjected to a detailed fissile lump analysis, which may be obtainable with a spatially sensitive passive neutron measurement proposed as part of the large crate-size passive neutron detector.[21] An x-ray analysis combined with one of the passive and/or active neutron measurements should also reveal the presence of a fissile lump. If a package containing a high TRU content contains a fissile lump, special handling and disposal is required. *Under no circumstances* should a lump (≥200 g of fissile material in a single piece) be allowed to enter the SPI Facility. The potential for criticality, even with the preventative measure of $B_2O_3$ poisoning, is too great to think of processing it routinely through the slagger. The sudden introduction of a large lump could result in a very rapidly developing criticality hazard. It is an anomaly and must be processed separately.

If the high TRU package does not contain lumps of significant mass, then the package can be blended with the appropriate volume of the low TRU fraction to generate an acceptable average TRU mix that can then be introduced safely into the SPI Facility.

The preliminary screening phase is not a high-quality assay measurement; ±50-100% quality is adequate. This can be done very rapidly (<100 s for packages up to and including crate size) and need not introduce any significant time delays in the overall processing. A more accurate (better geometry, better matrix compensation, etc.) assay measurement for the input/output considerations is best done with the final blended SPI Facility input material.

## IV. ASSAY OF PRODUCT SLAG CASTINGS

If $1.0 \times 10^{-2}$ wt fraction of $B_2O_3$ is added to the SPI Facility waste input, a fairly accurate assay of the final 91.44-cm-(36-in.-) diam x 30.48-cm-(12-in.-) thick, $\rho$ = 2.8-3.0 g/cm$^3$, slag casting is obtainable by simple total neutron counting. (Refer to Table IX.) The known $B_2O_3$ content of the slag casting should generate a fairly constant B($\alpha$,n) neutron source on a fixed neutron per alpha-particle basis. This is based on the fact that thick target neutron yields are not much different for the different alpha-particles that exist in the typical TRU wastes the SPI Facility will be processing (that is, the U, Pu, and Am isotopes). Thus, the final slag casting neutron output will be a quantitative indication of its total TRU content.

If a total fissile content is desired, we recommend an active neutron measurement. Considering the expected uniformity of the final product, any of the techniques discussed earlier could provide this assay. This measurement will be the easiest and by far the most accurate of all the measurements performed at the SPI Facility. We do not see a need for slag grab sample assays. The slag casting can be more than adequately assayed with presently known techniques.

## V. CONCLUSIONS, RECOMMENDATIONS, AND COST ESTIMATES

### A. Conclusions

We conclude on the basis of this study that the proposed SPI Facility will have a minimal criticality hazard associated with its operation if a three-level criticality-hazard prevention program is implemented. The three levels of the program are as follows.

1. A prescreening (50-100% accuracy, active neutron assay) of all incoming wastes is performed before they enter the SPI Facility processing stream. On the basis of this prescreening into three broad categories (each category to cover a factor of 3-10 or greater in fissile material concentration), only an average fissile concentration waste stream is processed by the SPI Facility. No significant fissile lumps or high-concentration fissile materials are allowed into the SPI Facility. This prevents a rapidly developing criticality hazard under most situations.

2. An approximate $1.0 \times 10^{-2}$ wt fraction of $B_2O_3$ (or equivalent neutron poison) mixture is added uniformly to all waste. This significantly improves the criticality safety while not significantly impacting processing volume or overall SPI Facility economics.

3. Direct criticality-hazard monitors are installed around the drying, pyrolysis, and slag forming regions and any other structure of the SPI Facility with a potential criticality hazard. These monitors should be based on passive neutron counting using an existing detector design. An adjunct active neutron system can be provided for monitoring the build-up of fissile isotopes.

We feel these three independent criticality-hazard prevention measures will lower the criticality hazard to an acceptably low level. At the same time, these three strategies do not add significantly to the cost or efficiency of the operation of the SPI Facility.

### B. Recommendations

Each of the three measures recommended requires more detailed study before actual start up of the SPI Facility. It is our judgment that the facility parameters (the size and shape of the drying and pyrolysis regions; composition of waste; detailed incinerator properties such as temperature and $B_2O_3$ distributions expected; and many other factors) need to be quantified beyond the present study. The final system will probably be somewhat different from that used in this study.

### C. Cost Estimates

Recommendations of specific instrumentation for the SPI Facility are based on the current (February 1980) state-of-the-art technology and on the authors' projections of what pertinent developments are likely to occur in the next few years.

1. The direct criticality monitors should be based on $^3$He/polyethylene open-faced sandwich proportional counter systems. A separate system will be required for each of the drying, pyrolysis, and slag regions. This is based on the MCNP calculational results that showed neutronic decoupling of these regions. Some development of these systems is required, chiefly, experimental/calculational determination of exact size requirements, as well as a more detailed study of the false alarm/optimal sensitivity problem. We estimate that monitor development costs will be about $200k in 1980 dollars. Equipment costs (these are more uncertain because exact detector sizes must be determined) for three separate systems with associated alarming equipment will likely be in the $300-$500k range (1980 dollars). This cost does not include the price of any SPI Facility system shutdown equipment. The active neutron addition discussed in the text would add about $50k to the cost of each system.

2. For the prescreening phase, we recommend an active neutron system, specifically, the DDT system because of its more rapid assay capability. We assume that this system's development will occur independently of the SPI Facility needs so that no developmental costs are included. (If more rapid system development is required for the SPI Facility, additional funds for this would be required.) Projected costs for a single large DDT system [to handle any waste package of 121.92 cm (48 in.) x 121.92 cm (48 in.) x 213.36 cm (84 in.) or smaller] will be about $300k, which includes a spare neutron generator and pulse transformer as well as all required personnel shielding. (The basic radiation hazard of this system is not large.) We assume that manual handling of waste packages with fork lifts or the like can be used. If fully automated handling is required, additional costs will be incurred.

3. For x-ray and other special measurements required for the few "problem" waste packages in the prescreening phase, we recommend a small, low-energy electron linac. Varian Associates of Palo Alto, California, produce, on a commercial basis, such linacs for medical and quality control x-ray work. A suitable 8-MeV machine (with pushbutton 6-, 8-, and 10-MeV options) is available from Varian Associates (linatron 2000) for about $300k on an operational basis. We recommend installing this in an outbuilding (a dirt-shielded, large-diameter cement drain culvert could be used to greatly reduce costs) rather than incorporating it into the SPI Facility.

4. A large passive neutron coincidence system may be desirable as part of the "problem" waste package measurements. This could be used to independently determine plutonium mass and possibly to provide lump detection and location. Because this system would be intended for use with relatively large plutonium masses (>10 g Pu), no elaborate cosmic-ray shielding is required. We estimate a system cost (no development costs included) of about $350k.

5. A separate (and smaller) DDT active neutron system would be required for final product slag casting assay. This system should cost about $200k.

6. For the highly accurate (5-10% accuracy) blended waste assay measurement done within the SPI Facility to provide input/output fissile information (if required), we recommend a separate, specially designed DDT system. For this purpose, special matrix compensation techniques will probably be required so that a highly accurate assay can be obtained. We estimate a $200-$300k development charge and a final design system cost of about $300k.

## ACKNOWLEDGMENT

We thank D. R. Smith and T. McLaughlin of the Los Alamos Scientific Laboratory for several helpful suggestions and for reviewing the manuscript.

## REFERENCES

1. "Use of Borosilicate Glass Raschig Rings as a Neutron Absorber in Solutions of Fissile Material," American National Standard, ANSI N16.4 (1971).

2. LASL Group X-6, W. L. Thompson, Ed., "MCNP—A General Monte Carlo Code for Neutron and Photon Transport," Los Alamos Scientific Laboratory report LA-7396-M, Rev. (November 1979).

3. Kaiser Engineers, Inc., "Preliminary Criticality Evaluation of SPI Gasifier and Secondary Combustion Chamber," Idaho National Engineering Laboratory report 79-24-R (April 1979).

4. Kirk McKinley, EG&G Idaho, Inc., private communication, November 1979.

5. "Gasifier Design Concept," The Ralph M. Parsons Company project number 961-006-80, drawing number 61006-D-10-000-01 (September 27, 1979).

6. "Secondary Combustion Chamber General Arrangement," The Ralph M. Parsons Company project number 961-006-80, drawing number 61006-D-20-000-01 (September 27, 1979).

7. H. F. Atwater, Los Alamos Scientific Laboratory, private communication.

8. F. deHoffman, "Statistical Aspects of Pile Theory," *The Science and Engineering of Nuclear Power, Vol. II,* C. Goodman, Ed. (Addison-Wesley Publishing Co., Inc., Massachusetts, 1949), pp.103-119.

9. J. Orndoff, "Prompt Neutron Periods of Metal Critical Assemblies," Nucl. Sci. and Eng. 2, 450 (1957).

10. S. H. Vegors, Jr., and E. B. Nieschmidt, "Preliminary Investigation of a Criticality Monitoring Technique for a Transuranic Waste Incinerator," Idaho National Engineering Laboratory report TREE-1285 (October 1978).

11. R. H. Augustson and T. D. Reilly, "Fundamentals of Passive Nondestructive Assay of Fissionable Material," Los Alamos Scientific Laboratory report LA-5651-M (September 1974).

12. N. Ensslin, M. L. Evans, H. O. Menlove, and J. E. Swanson, "Neutron Coincidence Counters for Plutonium Measurements," J. Inst. Nucl. Mater. Manage. INMM VII, 43 (Summer 1978).

13. K. P. Lambert and J. W. Leake, "A Comparison of the V.D.C. and Shift Register Neutron Coincidence Systems for $^{240}$Pu Assay," J. Inst. Nucl. Mater. Manage. INMM VII, 87 (Winter 1978-1979).

14. E. J. Dowdy, C. N. Henry, A. A. Robba, and J. C. Pratt, "New Neutron Correlation Measurement Technique for Special Nuclear Material Assay and Accountability," Proceedings of the International Symposium on Nuclear Material Safeguards, Vienna, Austria, October 2-6, 1978 (IAEA, Vienna, May 1979), Vol. II, pp. 125-136.

15. C. D. Ethridge, E. J. Dowdy, C. N. Henry, and D. R. Millegan, "A Microprocessor Based Neutron Count Moment Logic Module for Special Nuclear Material Assay by the Neutron Fluctuation Method," Proceedings ESARDA First Annual Symposium on Safeguards and Nuclear Material Management, Brussels, Belgium, April 25-26, 1979 (Brussels, 1979), pp. 320-324.

16. E. J. Dowdy, G. E. Hansen, A. A. Robba, and J. C. Pratt, "Effect of (α,n) Contaminants and Sample Multiplication on Statistical Neutron Correlation Measurements," Proceedings ESARDA Second Annual Symposium on Safeguards and Nuclear Material Management, L. Stanchi, Ed., Edinburgh, Scotland, March 26-28, 1980 (Edinburgh, 1980), pp. 359-363.

17. W. E. Kunz, J. D. Atencio, and J. T. Caldwell, "A 1-nCi/g Sensitivity Transuranic Waste Assay System Using Pulsed Neutron Interrogation," submitted to the Twenty-first Annual Meeting of the INMM, Palm Beach, Florida, June 30, July 1-2, 1980.

18. T. W. Crane, "Measurement of Pu Contamination at the 10-nCi/g Level in 55-Gallon Barrels of Solid Waste with a $^{252}$Cf Assay System," Proceedings of the International Meeting on Monitoring of Pu-Contaminated Waste, J. Ley, Ed., Ispra, Italy, September 25-28, 1979 (Ispra, 1980), pp. 217-226.

19. M. R. Cates, "Application of Linear Accelerator Technology to the Detection of Trace Amounts of Transuranics in Waste Barrels," submitted to the Symposium on the Management of Alpha-Contaminated Wastes, Vienna, Austria, June 2-6, 1980.

20. G. Robert Keepin, Ed., "Nuclear Safeguards Research and Development Program Status Report, October-December 1979," Los Alamos Scientific Laboratory report LA-8241-PR (May 1980).

21. J. T. Caldwell, "High Density Waste Assay: Large Crate Counting via Passive Neutron Counting," submitted to the Symposium on the Management of Alpha-Contaminated Wastes, Vienna, Austria, June 2-6, 1980.

---

## APPENDIX
## SPI FACILITY GEOMETRY FOR MCNP

The MCNP code requires an explicit description of all surfaces in the geometrical model. This appendix supplies this information for the SPI Facility, excluding all secondary structures. Figures A-1—A-31 are a comprehensive set showing the incinerator in the yz, xz, and xy planes. Cuts in the yz plane at important x positions are shown in Figs. A-1—A-6; cuts in the xz plane at important y positions are shown in Figs. A-7—A-19; cuts in the xy plane at important z positions are shown in Figs. A-20—A-31. The small numbers appearing on the figures are surface numbers as required by MCNP to describe the geometry. Table A-I gives a complete listing of all the surfaces needed to describe the geometry. These are included for completeness and for the reader who wants to know the details of the geometry. These surfaces can be interpreted by referring to Ref. 2.

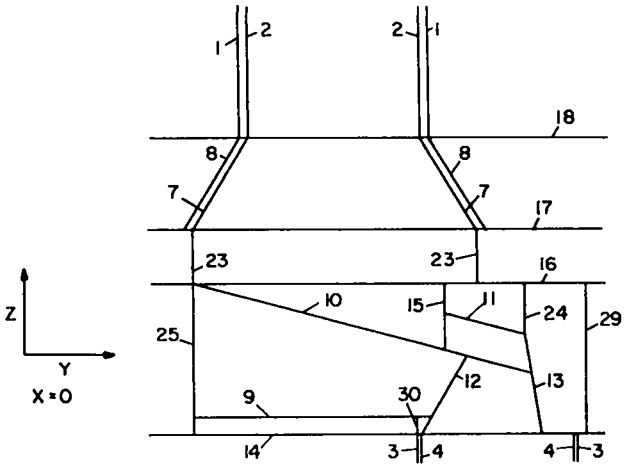


Fig. A-1.
View of the geometrical model of the SPI for the MCNP calculations. This is a cut in the yz plane at the point x = 0 cm.

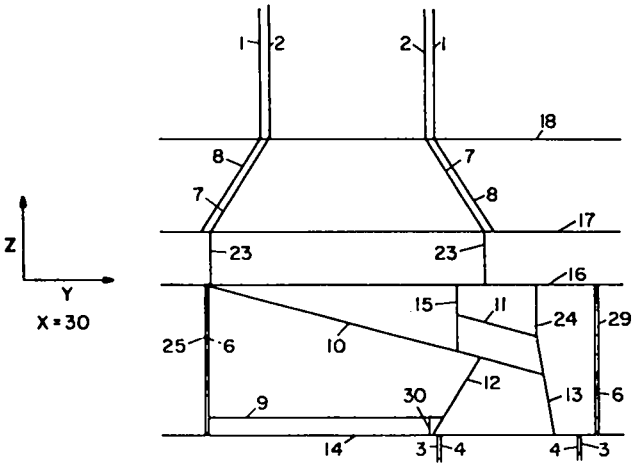


Fig. A-2.
View of the geometrical model of the SPI for the MCNP calculations. This is a cut in the yz plane at the point x = 30 cm.

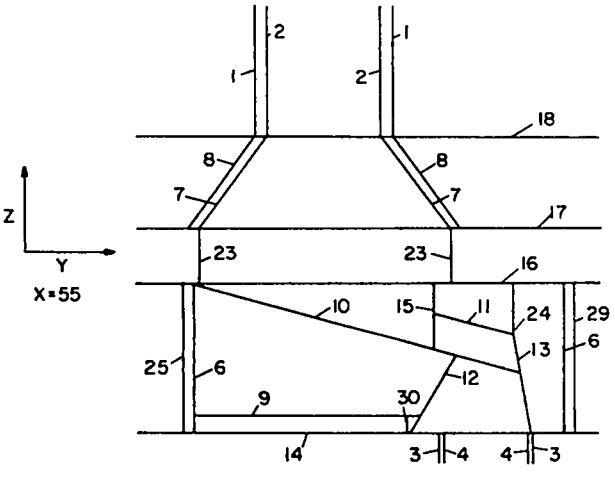


Fig. A-3.
View of the geometrical model of the SPI for the MCNP calculations. This is a cut in the yz plane at the point x = 55 cm.

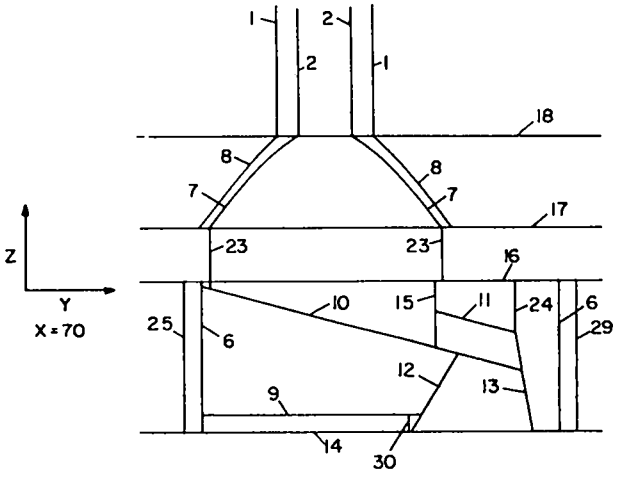


Fig. A-4.
View of the geometrical model of the SPI for the MCNP calculations. This is a cut in the yz plane at the point x = 70 cm.

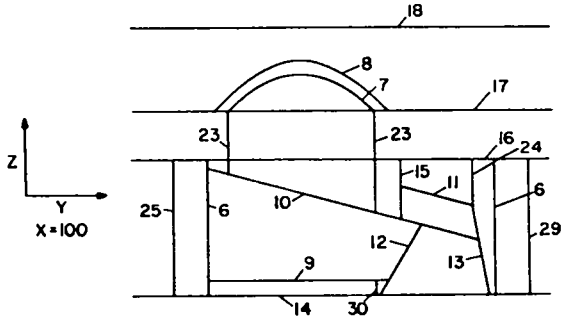


Fig. A-5.
View of the geometrical model of the SPI for the MCNP calculations. This is a cut in the yz plane at the point x = 100 cm.

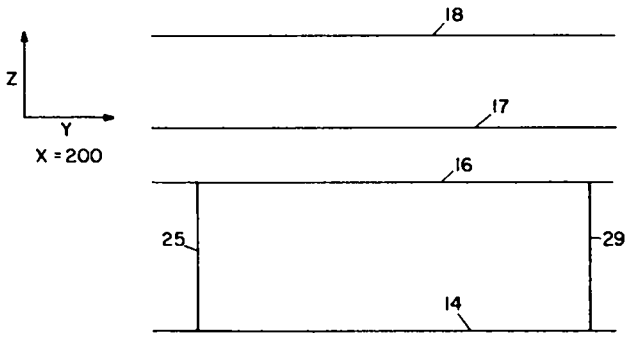


Fig. A-6.
View of the geometrical model of the SPI for the MCNP calculations. This is a cut in the yz plane at the point x = 200 cm.

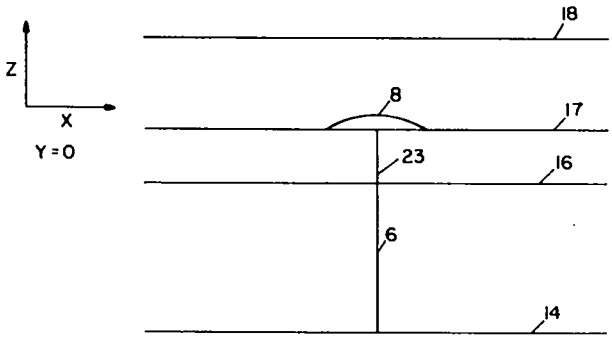


Fig. A-7.
View of the geometrical model of the SPI for the MCNP calculations. This is a cut in the xz plane at the point y = 0 cm.

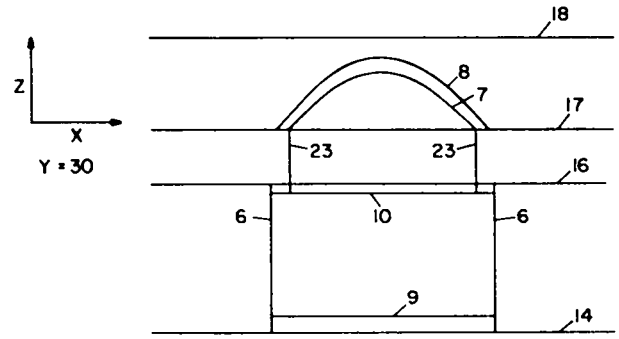


Fig. A-8.
View of the geometrical model of the SPI for the MCNP calculations. This is a cut in the xz plane at the point y = 30 cm.

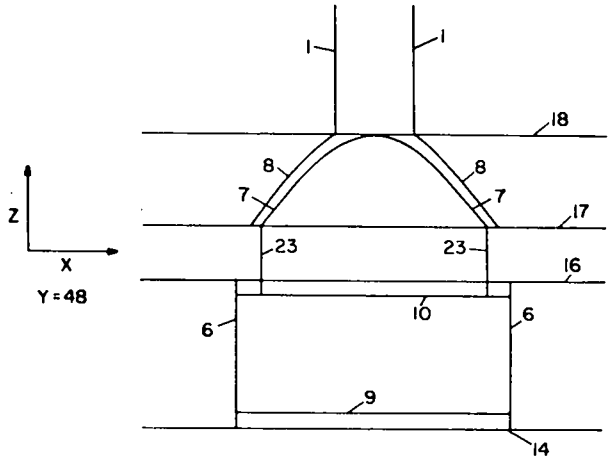


Fig. A-9.
View of the geometrical model of the SPI for the MCNP calculations. This is a cut in the xz plane at the point y = 48 cm.

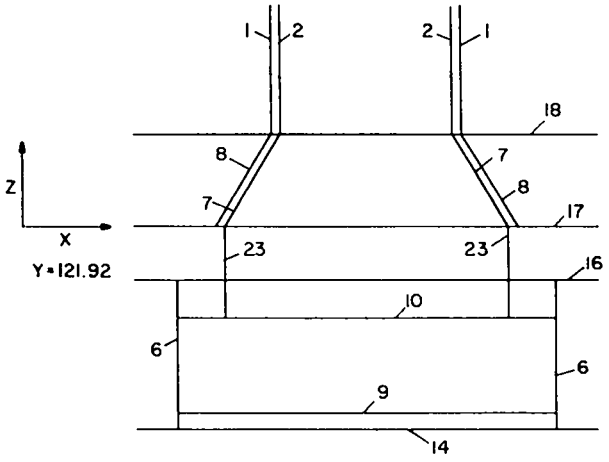


Fig. A-10.
View of the geometrical model of the SPI for the MCNP calculations. This is a cut in the xz plane at the point y = 121.92 cm.

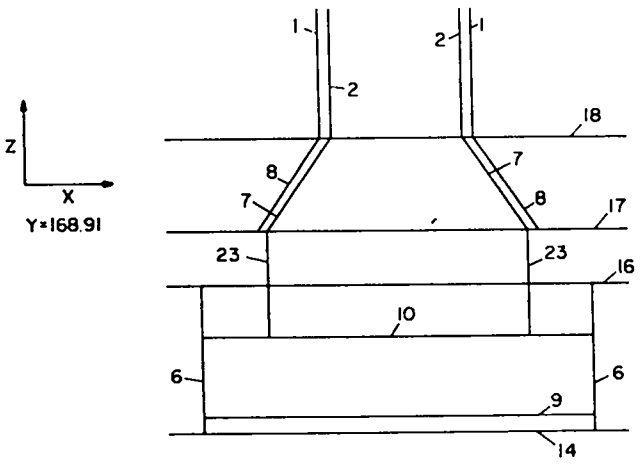


Fig. A-11.
View of the geometrical model of the SPI for the MCNP calculations. This is a cut in the xz plane at the point y = 168.91 cm.

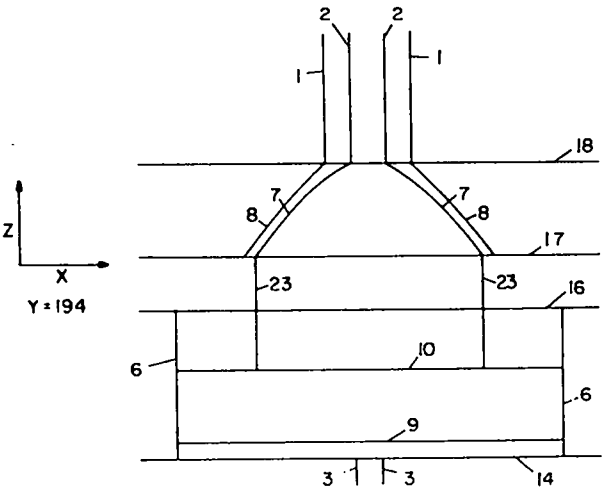


Fig. A-12.
View of the geometrical model of the SPI for the MCNP calculations. This is a cut in the xz plane at the point y = 194 cm.

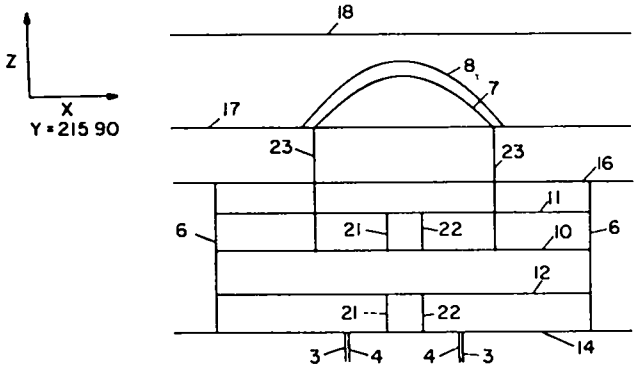


Fig. A-13.
View of the geometrical model of the SPI for the MCNP calculations. This is a cut in the xz plane at the point y = 215.90 cm.

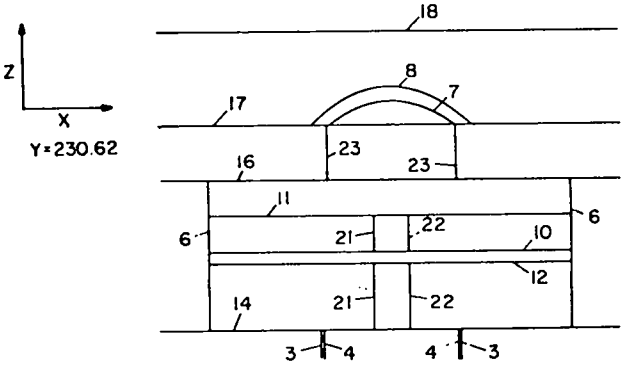


Fig. A-14.
View of the geometrical model of the SPI for the MCNP calculations. This is a cut in the xz plane at the point y = 230.62 cm.

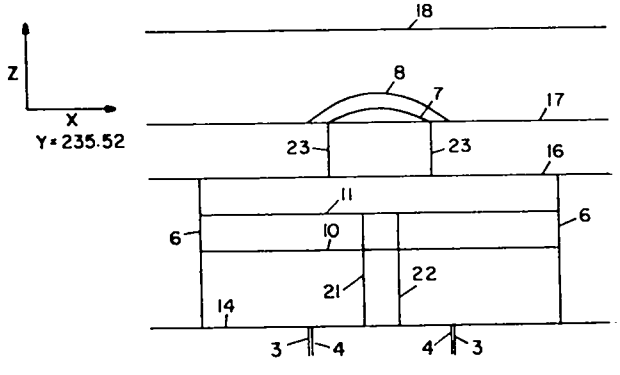


Fig. A-15.
View of the geometrical model of the SPI for the MCNP calculations. This is a cut in the xz plane at the point y = 235.52 cm.

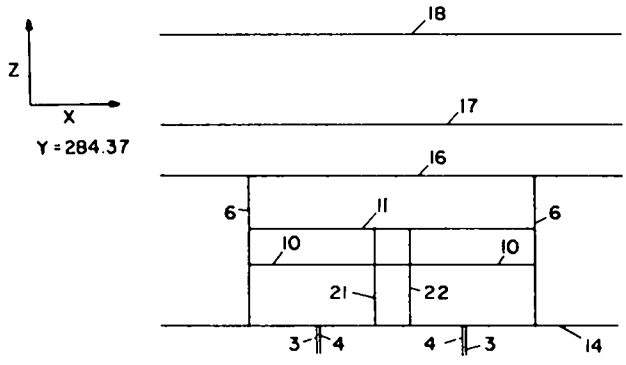


Fig. A-16.
View of the geometrical model of the SPI for the MCNP calculations. This is a cut in the xz plane at the point y = 284.37 cm.

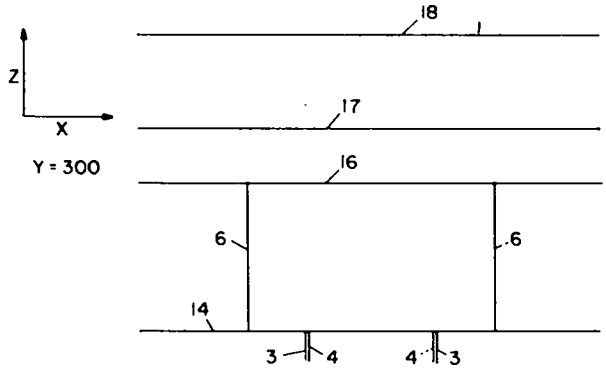


Fig. A-17.
View of the geometrical model of the SPI for the MCNP calculations. This is a cut in the xz plane at the point y = 300 cm.

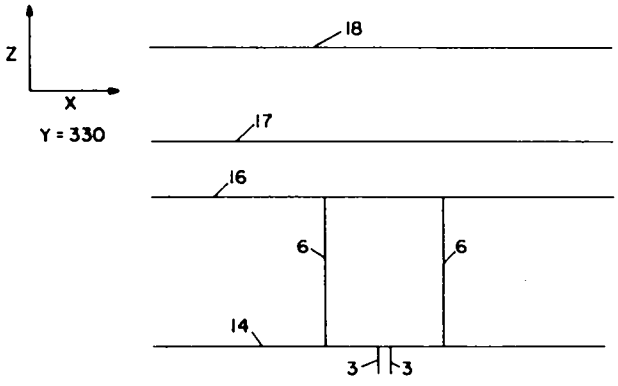


Fig. A-18.
View of the geometrical model of the SPI for the MCNP calculations. This is a cut in the xz plane at the point y = 330 cm.

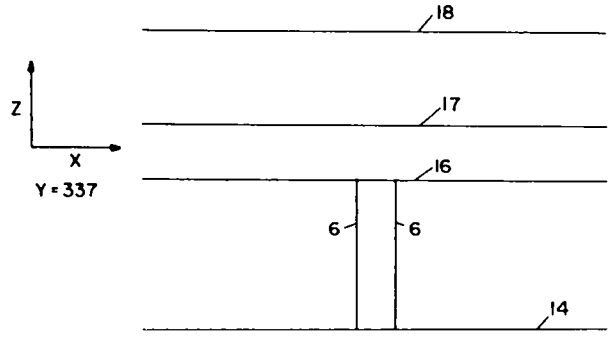


Fig. A-19.
View of the geometrical model of the SPI for the MCNP calculations. This is a cut in the xz plane at the point y = 337 cm.

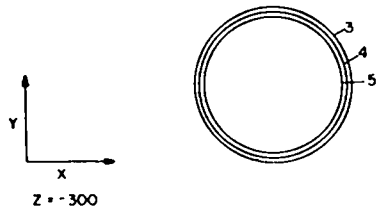


Fig. A-20.
View of the geometrical model of the SPI for the MCNP calculations. This is a cut in the xy plane at the point z = −300 cm.

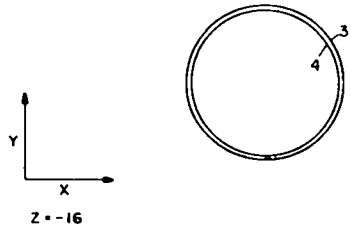


Fig. A-21.
View of the geometrical model of the SPI for the MCNP calculations. This is a cut in the xy plane at the point z = −16 cm.

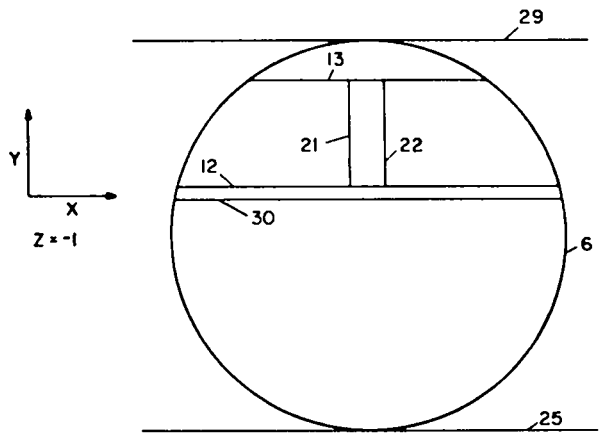


Fig. A-22.
View of the geometrical model of the SPI for the MCNP calculations. This is a cut in the xy plane at the point z = −1 cm.

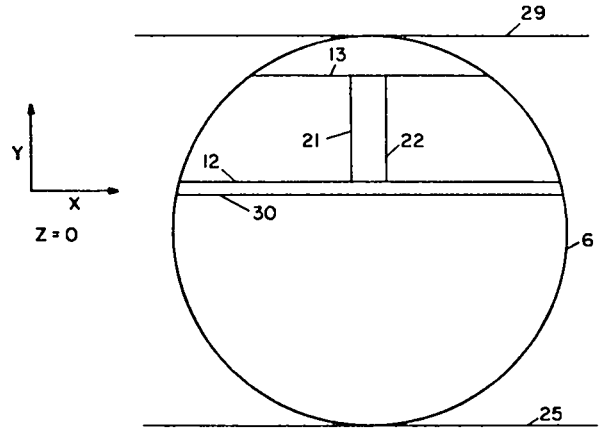


Fig. A-23.
View of the geometrical model of the SPI for the MCNP calculations. This is a cut in the xy plane at the point z = 0 cm.

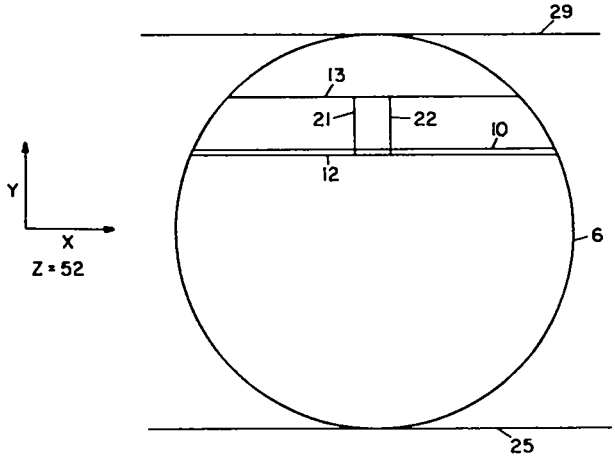


Fig. A-24.
View of the geometrical model of the SPI for the MCNP calculations. This is a cut in the xy plane at the point z = 52 cm.

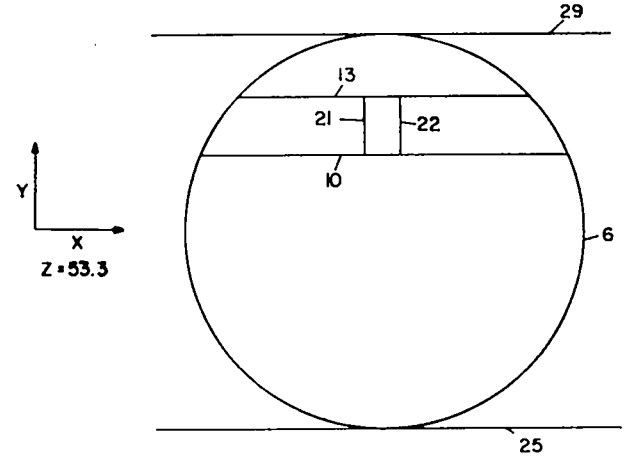


Fig. A-25.
View of the geometrical model of the SPI for the MCNP calculations. This is a cut in the xy plane at the point z = 53.3 cm.

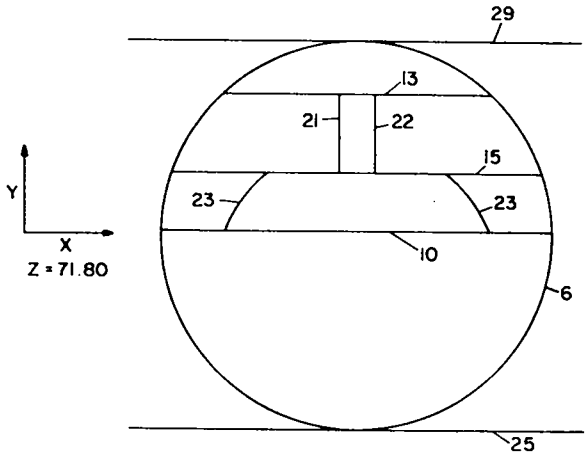


Fig. A-26.
View of the geometrical model of the SPI for the MCNP calculations. This is a cut in the xy plane at the point z = 71.80 cm.

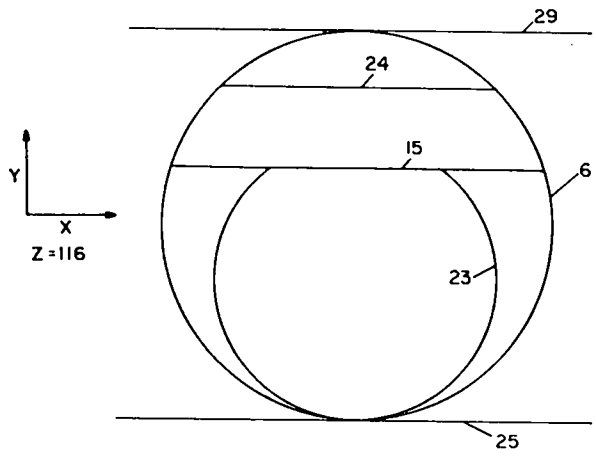


Fig. A-27.
View of the geometrical model of the SPI for the MCNP calculations. This is a cut in the xy plane at the point z = 116 cm.

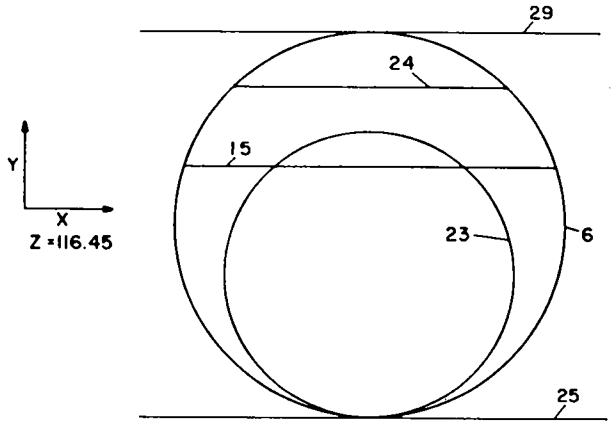


Fig. A-28.
View of the geometrical model of the SPI for the MCNP calculations. This is a cut in the xy plane at the point z = 116.45 cm.

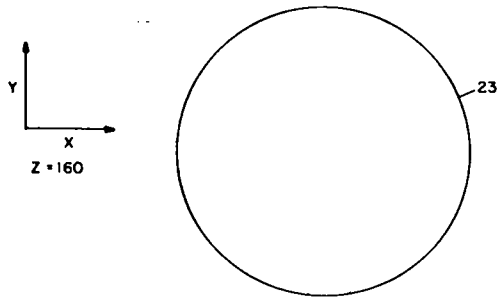


Fig. A-29.
View of the geometrical model of the SPI for the MCNP calculations. This is a cut in the xy plane at the point z = 160 cm.

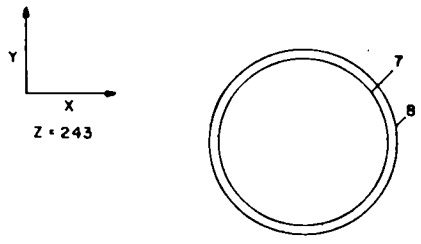


Fig. A-30.
View of the geometrical model of the SPI for the MCNP calculations. This is a cut in the xy plane at the point z = 243 cm.

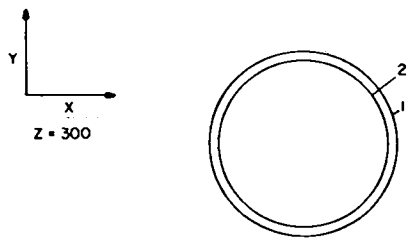


Fig. A-31.
View of the geometrical model of the SPI for the MCNP calculations. This is a cut in the xy plane at the point z = 300 cm.

TABLE A-I

GEOMETRY OF INCINERATOR

```
 1 C/Z 0 121.92 81.28
 2 C/Z 0 121.92 73.66
 3 C/Z 0 261.62 68.58
 4 C/Z 0 261.62 66.04
 5 C/Z 0 261.62 60.96
 6 C/Z 0 168.91 168.91
 7 K/Z 0 121.92 365.9605263 0.3638196019E-1
 8 K/Z 0 121.92 378.5936842 0.3638196019E-1
 9 PZ 0
10 P 0 2.300980615E-3 8.587376556E-3 1
11 P 0 2.300980615E-3 8.587376556E-3 1.2709765391
12 P 0 1.732050806E-1 354.6052253
13 P 0 3.366631827E-3 5.936280184E-4 1
14 PZ -15.24
15 PY 215.90
16 PZ 116.45
17 PZ 163.83
18 PZ 243.84
19 PZ 612.14
20 PZ 868.68
21 PX -15.24
22 PX 15.24
23 C/Z 0 121.92 121.92
24 PY 284.3710495
25 PY 0
26 PZ -106.68
27 PZ -191.44
28 PZ -282.88
29 PY 337.82
30 PY 193.04
31 C/Z 0 261.62 3000
32 PZ -100.00
33 SO 13000000
34 PZ 335.27
```

Printed in the United States of America
Available from
National Technical Information Service
US Department of Commerce
5285 Port Royal Road
Springfield, VA 22161

Microfiche $3.50 (A01)

| Page Range | Domestic Price | NTIS Price Code | Page Range | Domestic Price | NTIS Price Code | Page Range | Domestic Price | NTIS Price Code | Page Range | Domestic Price | NTIS Price Code |
|---|---|---|---|---|---|---|---|---|---|---|---|
| 001-025 | $ 5.00 | A02 | 151-175 | $11.00 | A08 | 301-325 | $17.00 | A14 | 451-475 | $23.00 | A20 |
| 026-050 | 6.00 | A03 | 176-200 | 12.00 | A09 | 326-350 | 18.00 | A15 | 476-500 | 24.00 | A21 |
| 051-075 | 7.00 | A04 | 201-225 | 13.00 | A10 | 351-375 | 19.00 | A16 | 501-525 | 25.00 | A22 |
| 076-100 | 8.00 | A05 | 226-250 | 14.00 | A11 | 376-400 | 20.00 | A17 | 526-550 | 26.00 | A23 |
| 101-125 | 9.00 | A06 | 251-275 | 15.00 | A12 | 401-425 | 21.00 | A18 | 551-575 | 27.00 | A24 |
| 126-150 | 10.00 | A07 | 276-300 | 16.00 | A13 | 426-450 | 22.00 | A19 | 576-600 | 28.00 | A25 |
| | | | | | | | | | 601-up | † | A99 |

†Add $1.00 for each additional 25-page increment or portion thereof from 601 pages up.